Am J Cancer Res 2023;13(11):5698-5718
www.ajcr.us /ISSN:2156-6976/ajcr0152616

Original Article

Suppression of alpha-tubulin acetylation potentiates therapeutic efficacy of Eribulin in liver cancer

Yiming Zhong[1,3*], Chaoqun Wang[2*], Yanmei Wang[3*], Yan Wu[1], Hanying Wang[3], Shuying Qiu[3], Minyan Hao[3], Zhuo Wang[3], Xian Wang[3], Hongchuan Jin[1], Jia Zhou[1,3]

[1]Laboratory of Cancer Biology, Key Lab of Biotherapy in Zhejiang Province, Cancer Center of Zhejiang University, Sir Run Run Shaw Hospital, School of Medicine, Zhejiang University, Hangzhou 310016, Zhejiang, China; [2]Department of Pathology, Affiliated Dongyang Hospital of Wenzhou Medical University, Dongyang 322100, Zhejiang, China; [3]Department of Medical Oncology, Sir Run Run Shaw Hospital, School of Medicine, Zhejiang University, Hangzhou 310016, Zhejiang, China. [*]Equal contributors.

Received August 4, 2023; Accepted October 25, 2023; Epub November 15, 2023; Published November 30, 2023

Abstract: Hepatocellular carcinoma (HCC) is a prevalent cancer with limited effective treatments. Eribulin mesylate is a novel chemotherapy drug that inhibits microtubule elongation and may impact the tumor microenvironment and immune pathway. This study aims to investigate the impact of changes in microtubule acetylation levels on HCC development and treatment outcomes. Clinical and molecular data were aggregated from databases, with survival analysis conducted to evaluate the relevance of microtubule acetylation. *In vitro* experiments using HCC cell lines and a tumor cell transplantation model in C57BL/c mice were performed to investigate the effects of microtubule acetylation on Eribulin treatment. A significant correlation was found between the level of lysine 40 acetylation of α-tubulin (acetyl-α-tubulin-lys40) and overall survival of HCC patients, with a better prognosis associated with a lower level of acetyl-α-tubulin-lys40. Knocking down ATAT1 or overexpressing HDAC6 reduced the level of acetyl-α-tubulin-lys40 and sensitized Eribulin treatment both *in vitro* and *in vivo*. In summary, acetyl-α-tubulin-lys40 was increased in HCC and was associated with a shorter overall survival of HCC patients. Reducing the level of acetyl-α-tubulin-lys40 can enhance sensitivity to Eribulin treatment both *in vitro* and *in vivo*, thereby establishing acetyl-α-tubulin-lys40 as a potential prognostic marker and predictive indicator for Eribulin treatment in HCC patients.

Keywords: Eribulin mesylate, hepatocellular carcinoma, microtubule acetylation modification, survival prognosis

Introduction

According to the Global Cancer Incidence, Mortality and Prevalence (GLOBOCAN) 2020 database version 1.0, hepatocellular carcinoma (HCC) is a malignant tumor with a notably high incidence and mortality worldwide. In 2020, HCC ranked sixth among all cancers in terms of incidence and was the third leading cause of cancer death globally, following lung and colorectal cancers [1]. In China, HCC incidence ranked second and seventh in males and females respectively, while mortality rates ranked second and fourth [2]. Recent statistical results have indicated that HCC patients in China often present with a higher proportion of advanced-stage disease at their initial clinical visit, with 1-, 3-, and 5-year survival rates for patients in stages III-IV being 68.50%, 47.00%, and 40.00% respectively [3]. Currently, HCC systemic therapy predominantly relies on molecular targeting, immunotherapy combined with anti-angiogenic therapy, and local treatment [4-9]. There are limited treatment options available after the emergence of treatment resistance [10, 11]. Chemotherapy for HCC patients is typically based on fluorouracil and platinum drugs, but traditional chemotherapy drugs have shown low efficacy. Taxanes, as representative drugs targeting microtubules, have demonstrated anti-tumor activity and improved prognosis in multiple tumor treatments, but their efficacy in HCC studies has been unsatisfactory [12, 13]. Due to the limited effective treatment options for advanced HCC, there is an urgency to explore more effective treatment methodologies [13-15]. A computational framework study, which mentioned

Eribulin as a potential drug for HCC treatment, piqued our interest [16].

Eribulin mesylate (also known as Halaven®, E7389, NSC 707389, ER-086526, hereafter referred to as Eribulin) is a novel microtubule-targeting anti-tumor drug, structurally modified from the marine natural product Halichondrin B following optimization [17, 18]. It has been approved for the treatment of metastatic breast cancer and liposarcoma [19-24]. Additionally, several studies have recently focused on Eribulin for therapeutic treatment of other tumor types such as uterine leiomyosarcoma, gastric cancer, colorectal cancer, and hematologic neoplasms [25-30]. Eribulin's pharmacological effect differs from other microtubule-targeting chemotherapy drugs, such as paclitaxel or vincristine [31-33], and has demonstrated particular efficacy in tumors that are insensitive to paclitaxel [17, 34]. *In vitro* experiments have shown that Eribulin has a more pronounced effect of inhibiting cell growth compared with other microtubule-targeting drugs [35]. Previous studies have indicated that its primary mechanism of action is to inhibit microtubule polymerization rather than depolymerization, leading to irreversible microtubule elongation arrest [36, 37]. Eribulin's mechanism of action also encompasses inhibition of microtubule spindle dynamics, mitotic arrest (G2-M phase cell cycle arrest), induction of apoptosis, and aggregation of non-productive microtubule proteins [35, 38, 39].

Microtubules, formed by the polymerization of α-tubulin and β-tubulin [40, 41], are the major components of the eukaryotic cell cytoskeleton. They play crucial roles in cytoskeleton formation, maintenance of cell shape, signal transduction, and mitosis, which are highly conserved through evolution [42, 43]. In cancer cells, microtubules participate in various physiological processes such as growth, proliferation, and migration [44-46]. Thus, microtubules are considered one of the critical targets in current anti-cancer drug development [42, 47]. Targeting microtubules can affect their assembly or disassembly, effectively disrupting microtubule dynamics, further interfering with cell mitosis and spindle formation, and ultimately inducing apoptosis [48-51]. Numerous post-translational modifications (PTMs) occur on microtubule proteins, including acetylation, polysaccharide glycosylation, polyglutamylation, and tyrosination, which significantly impact microtubule assembly, structure, and stability [52, 53] and play vital roles in the development of some human diseases, including tumorigenesis [54, 55]. Currently, limited research exists on the functional role of microtubule acetylation in cells [54]. Lysine acetylation modification on microtubule proteins was first discovered in 1983 [56, 57], and this modification has been found to be a conserved PTM in evolution [58]. The lysine at position 40 of α-tubulin can be acetylated by cytoplasmic acetyltransferase ATAT1 (Alpha Tubulin Acetyltransferase 1) [59] and deacetylated by cytoplasmic deacetylase HDAC6 (Histone Deacetylase 6) [60, 61]. Studies have revealed that HDAC6 can deacetylate α-tubulin and induce microtubule depolymerization, resulting in microtubule instability [62]. ATAT1, having a high affinity for microtubules, can effectively catalyze microtubule protein acetylation [63]. It can also be regarded as a "slow clock" for the microtubule lifespan [63]. Depletion of ATAT1 increases the frequency of mechanical stress-induced microtubule breakage [64]. The above studies suggest that acetylation increases the mechanical elasticity of microtubules, enhances their flexibility and resilience against mechanical breakage, and ensures their long-term lifespan [63, 65]. Apart from increasing the microtubule stability, the role of microtubules acetylation modification in cancer and chemotherapy resistance still needs to be further explored.

This study aims to explore the efficacy and mechanism of action of Eribulin in HCC and provide new strategies for the treatment of HCC. We found that high level of acetyl-α-tubulin-lys40 correlated with a poor survival prognosis in HCC patients, and decreasing the level of acetylation modification of microtubules could enhance the sensitivity of Eribulin both *in vitro and in vivo*.

Materials and methods

Cell culture

All cells in this experiment were cultured in DMEM medium containing 10% FBS and 1% penicillin/streptomycin, and were maintained in a cell culture incubator at 37°C with 5% CO_2.

Animal experiments

The experimental mice used in the animal experiments were C57BL/6 mice, 5 to 6-week-old, weighing 16-20 g. They were purchased and housed at the Experimental Animal Center of Sir Run Run Shaw Hospital, Zhejiang University School of Medicine. The animal facility of the Experimental Animal Center is at SPF level, with a room temperature of 23-25°C, humidity of 67%-75%, light from 7:00 to 21:00 and darkness from 21:00 to 7:00 the next day, and a light/dark cycle ratio of 14 h/10 h. Mice were provided with unlimited access to food and water. All animal experimental protocols in this study were approved by the Animal Ethics Committee of Sir Run Run Shaw Hospital, Zhejiang University School of Medicine.

The mice were transplanted with the Hepa1-6 knockdown Atat1 stable transfection strain and the overexpression Hdac6 stable transfection strain into the mice subcutaneously at the number of 2×10^5 cells per mouse to establish mice tumor cell transplantation model, and subsequent treatment with Eribulin. The dosage of treatment was 6.3 μg Eribulin/20 g mouse everyday (refer to 2.3 Dosage calculation for detail). The cells were transplanted in the right armpit of the mice on day 0, then the mice were randomly divided into two groups according to their body weight, and the therapy began on the 1st day after the subcutaneous injection (the treatment group received intraperitoneal injection of Eribulin, and the control group received intraperitoneal injection of normal saline at the same dose according to the body weight). The body weight and subcutaneous tumor size of the mice were measured and recorded every day. The end point of the experiment: the size of the subcutaneous tumor reaching the ethical requirement, or there is a significant difference in the size of the subcutaneous tumor between the treatment group and the control group. After reaching the end point, the mice are humanely killed in a carbon dioxide environment, and the subcutaneous tumor is dissected.

Dosage calculation

According to the instructions of Eribulin, in breast cancer, the recommended dosage for a 70 kg adult (approximately 1.73 m^2 body surface area) is 1.4 mg/m^2, which is equivalent to 0.0346 mg/kg. In previous preclinical experiments, the dosages used for different tumor cell mouse transplantation models ranged from 0.125 mg/kg to 1 mg/kg [35]. In subsequent phase I clinical trials, the dosages used for HCC patients ranged from 0.25 mg/m^2 to 1.4 mg/m^2 [19, 20]. Based on experience pooled from multiple studies, the conversion ratio between mouse and human doses is 9.1:1 [66], the dosage for mice based on the recommended dosage in the package insert is approximately 0.315 mg/kg, which translates to 6.3 μg Eribulin/20 g mouse. This dosage is closer to the dosages used in preclinical experiments and clinical trials.

Proteomic and gene expression datasets

We downloaded gene expression data, mutational information, and clinical data for 365 liver hepatocellular carcinoma (LIHC) from The Cancer Genome Atlas (TCGA) network project via cbioportal online tool (available online: http://www.cbioportal.org/, accessed on May 1, 2022), proteomic data for 179 LIHC from The Cancer Proteome Atlas (TCPA) network project (available online: https://www.tcpaportal.org/, accessed on May 1, 2022).

Human tissue samples, immunohistochemistry

Surgical pathological samples of HCC patients were collected from the People's Hospital of Dongyang County, Zhejiang Province. All patients signed informed consent forms, and the sample collection was approved by the hospital's ethics review committee and followed the principles of the Helsinki Declaration. Immunohistochemistry results were completed by the pathology department. The result interpretation was as follows: unstained was 0, the most robust staining was 3+, and the intermediate levels were 1+ and 2+.

Protein extracts, western blot

The lysed cell extracts were adjusted to an appropriate concentration using a lysis buffer. Subsequently, a mixture of sample buffer and cell extracts was loaded onto a 10% SDS-polyacrylamide gel, and electrophoresis was run for 30 minutes at 80 volts, followed by 90 minutes at 120 volts. The PVDF membrane was then used for transfer, which was transformed at 120 mA for 120 minutes. Next, the

membrane was blocked with 5% non-fat milk in TBST for 60 minutes at room temperature, followed by incubation with the primary antibody at 4°C overnight. After washing thrice in TBST, the membrane was incubated with a secondary antibody for one hour at room temperature. Images were captured using the Amersham Imager 680 (GE, USA). The primary antibodies used in this study are listed below: anti-ATAT1 antibody (dilution 1:2000) (No. NBP2-48860, Novus Biologicals, USA); anti-acetyl-alpha tubulin (Lys40) antibody (dilution 1:2000) (No. 322700, life technologies, USA); anti-α-tubulin antibody (dilution 1:2000) (No. t5168, Sigma, USA); anti-GAPDH antibody (dilution 1:5000) (No. 2251-1, Epitomics, USA); anti-HDAC6 antibody (dilution 1:2000) (No. ET1701-66, HUAAN, China).

Cell viability assay

The Cell Counting Kit-8 assay (CCK-8, FDbio, Hangzhou, China) was conducted following the manufacturer's instructions. Briefly, 1×10^4 cells were seeded in a 96-well plate with 100 μL of medium and subjected to various treatments for specified durations, as detailed in the Results section. Afterward, 100 μL of 10% CCK-8 reagent was added and incubated at 37°C for 0.5~2 hours, and the absorbance was measured at 450 nm using a microplate reader. The differences in cell viability were examined. Each experiment would be conducted for at least three times of biological replications.

Drug-sensitive crystal violet staining

Uniformly seeded 2×10^5 cells into a 12-well plate, treated with different concentrations of Eribulin the following day, and stained the cells in the wells with crystal violet 48 hours later. Images were taken under a microscope and processed using ImageJ software.

Molecular cloning

Molecular cloning in cell experiments involves the construction of recombinant DNA expression vectors, plasmid transformation and identification, and plasmid amplification and extraction. Firstly, total RNA is extracted from cells, and cDNA is synthesized using reverse transcription PCR (RT-PCR). Using the designed primers for the corresponding gene fragment (i.e., upstream primer F and downstream primer R), the coding sequence of the gene region is PCR amplified using a high-fidelity DNA polymerase (Pfu Ultra II Fusion HS, Agilent, USA). After PCR, the product should be purified and recovered by gel electrophoresis separation according to the different molecular weight sizes and a DNA gel recovery kit (Gel DNA Recovery Kit, Zymoclean, China). The plasmid is constructed using double enzyme digestion, in which the cDNA fragment and the empty vector are subjected to double enzyme digestion to obtain linear DNA fragments with the same sticky ends, which are then recovered by gel electrophoresis. The target plasmid is transformed, identified, and amplified using DH5α competent E. coli (Weidibio, China) as a vector. HDAC6 primer: Upstream primer F: 5'-GGCTAGCGCCACCATGACCTCAACCGGCCAGGA-3', Downstream primer R: 5'-CGGATCCTTAGTGTGGGTGGGGCATATCCTCC-3'.

Generation of ATAT1-knockdown and HDAC6-overexpressing cell lines

To knockdown ATAT1 gene (ATAT1-KD) in HCC cell lines, small interfering RNA (siRNA) transfection experiments are performed using the following siRNA (GenePharma, China): siControl (silencer select negative control), siATAT1 #1 (sense: 5'-GCCAAGGCCCAGAAUCUUUTT-3', antisense: 5'-AAAGAUUCUGGGCCUUGGCTT-3', GenePharma, China), siATAT1 #2 (sense: 5'-GGAUGAUCGUGAGGCUCAUTT-3', antisense: 5'-AUGAGCCUCACGAUCAUCCTT-3', GenePharma, China). Lipofectamine RNAiMAX (ThermoFisher SCIENTIFIC, USA) is used as transfection reagent.

The HDAC6-overexpressing (HDAC6-OE) cell lines are stable cell lines constructed by lentiviral vector infection, and the plasmids are constructed by "Molecular cloning" described above.

Cellular immunofluorescence assay

Target cells are seeded in a 12-well or 24-well plate with cell culture slides before the experiment, with a cell density of 50% to 70% on the day of slide preparation. The cell culture slides are washed three times with 1 × PBS, fixed with 4% paraformaldehyde for 30 minutes, washed three times with 1 × PBST, and blocked with 5% BSA for 30 minutes. The primary anti-

body is diluted in 5% BSA and incubated overnight at 4°C, followed by washing and incubation with the secondary antibody at room temperature for 1 hour. The cell nuclei are stained with DAPI and washed. The slides are sealed with the anti-fluorescent quencher. Images are captured using a fluorescence-inverted microscope.

Cell apoptosis detection

The Annexin V-FITC/PI apoptosis kit (Lianke Biology, China) was used to detect cell apoptosis levels. Cells were seeded into a 12-well plate, treated accordingly, and then collected and processed according to the kit instructions. Cell apoptosis was detected using a flow cytometer, and FlowJo software (version 10.8.1) was used for analysis.

Cell cycle detection

The Cell Cycle Staining Kit (by LIANKO, China) was used to detect cell cycle distribution. Cells were seeded in a 12-well plate, treated accordingly, and collected and processed according to the manufacturer's instructions. Cell cycle detection was performed using a flow cytometer, and the data were analyzed using ModFit (version 3.0).

Microtubule aggregation semi-quantitative detection

The Cytoskeleton #BK004P kit was used to perform microtubule aggregation semi-quantitative detection. The microtubule protein buffer and paclitaxel positive control reagents were prepared according to the kit instructions. The drug at the appropriate concentration to be tested was selected, and a 100 μL reaction system was equipped and added to the 96-well plate provided in the kit. The absorbance was measured every 30 seconds at 37°C, and 121 data points were collected over 60 minutes, including the initial reading at time 0. The absorbance data were processed and plotted to generate a curve showing the change in absorbance over time.

Survival analysis

Survival analysis was performed based on data from TCGA, TCPA, and clinical follow-up data. The R packages "survival", "survminer", "RColorBrewer", "dplyr", "plyr", "glmnet", "rms", "VIM", etc. were used to analyze survival, draw survival curves, perform Cox regression analysis, calculate and draw column charts, and so on.

Statistical analysis

All statistical analyses in this study were performed using GraphPad Prism (version 9.5.1) software and R (version 4.1.0), with R running in the RStudio (version 2022.02.3+492) environment. The results were analyzed by non-paired Student's t-test, one-way ANOVA, two-way ANOVA, and χ^2 (and Fisher's exact) test. Univariate and multivariate Cox regression analyses were employed to evaluate the impact of relevant factors on survival prognosis. Kaplan-Meier survival curve analysis was used to compare survival differences between different groups. Each experiment was independently repeated at least three times. Significance level was represented by *p*-values, with "*" indicating $P < 0.05$, "**" indicating $P < 0.01$, "***" indicating $P < 0.001$, and "****" indicating $P < 0.0001$.

Results

High level of acetyl-α-tubulin-lys40 is correlated with poor prognosis of HCC patients

We downloaded the reverse protein array (RPPA) level 4 data for 179 LIHC samples from HCC patients from the TCPA and standardized the data to obtain basic patient information (Supplementary Table 1). We selected data containing patient IDs, levels of acetyl-α-tubulin-lys40, patient survival time, and survival status. Using R, we calculated the optimal cutoff point for the level of acetyl-α-tubulin-lys40 to be -0.2184. We divided the data into high- and low-level groups based on this cutoff value and found a significant correlation between the level of acetyl-α-tubulin-lys40 and patient prognosis through further analysis of the overall survival (OS) of patients in each group (**Figure 1A**). A high level of acetyl-α-tubulin-lys40 was associated with shorter overall survival, indicating that acetyl-α-tubulin-lys40 might be an applicable prognostic biomarker in HCC.

A further stratified analysis of the TCPA database calculated OS curves for acetyl-α-tubulin-

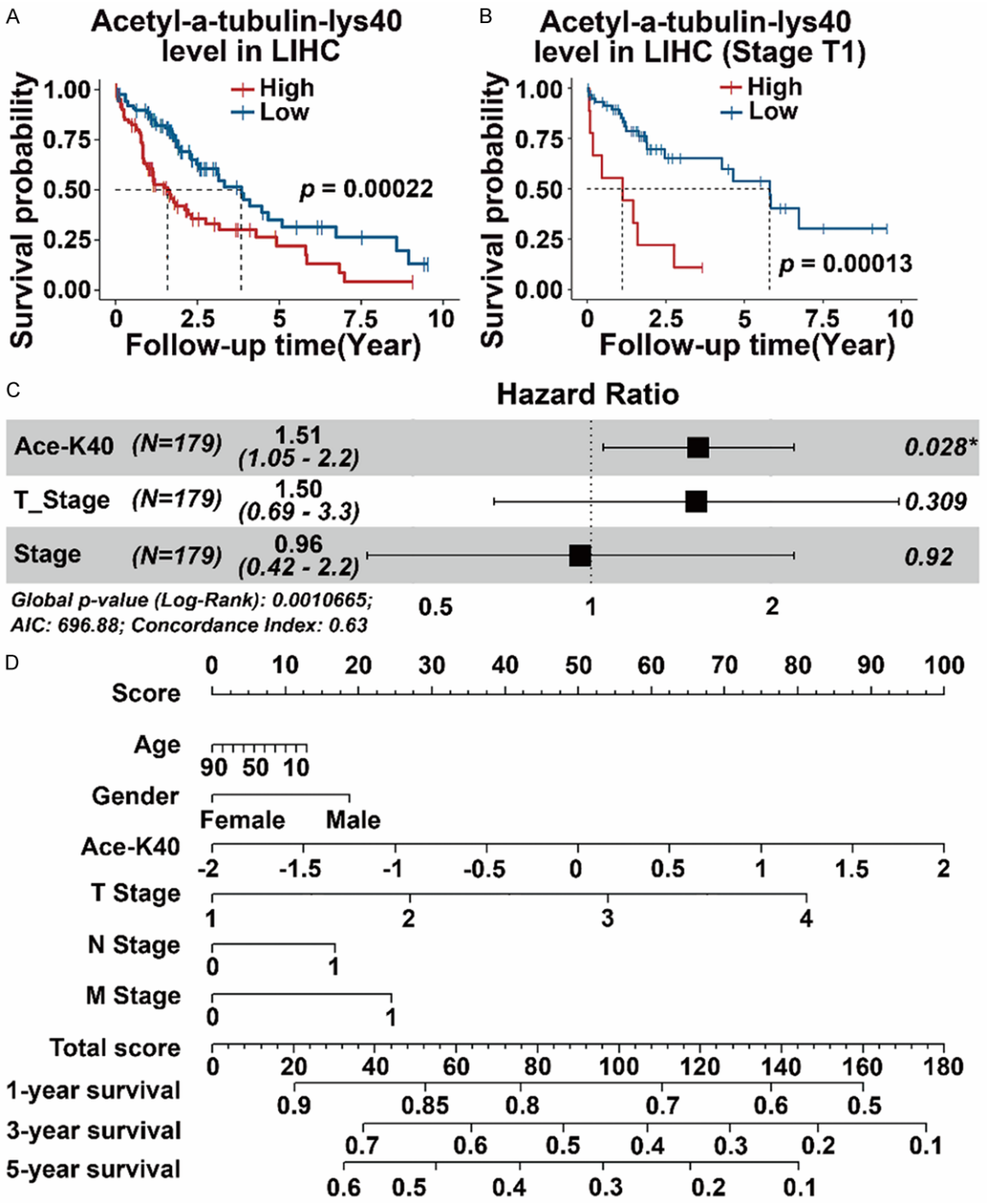

Figure 1. High level of acetyl-α-tubulin-lys40 correlated with poor prognosis in HCC patients. A. Overall survival (OS) analysis was performed on acetyl-a-tubulin-lys40 in HCC patients using data from the TCPA database, with a cutoff value of -0.2184 and *P* = 0.00022, showing significant differences; B. Survival curve for T1 stage HCC patients with a cutoff of 0.152 and *P* = 0.00013; C. Multivariate Cox regression analysis was performed by a forest plot. The level of acetyl-α-tubulin-lys40 was identified as an independent risk factor for OS of HCC patients (*P* = 0.028); D. The nomogram was constructed based on data from TCGA and TCPA database to predict 1, 3, 5-year survival of LIHC.

lys40 levels in HCC patients at different stages (**Figure 1B**, Supplementary Figure 1A-C). We excluded N1 and M1 stage patients from this survival analysis due to the potential for signifi-

Table 1. Univariate and multivariate Cox regression analysis of LIHC patients

Group	Univariate Cox			Multivariate Cox		
	HR	CI95	*p*	HR	CI95	*p*
Acetyl-α-tubulin-lys40	1.55	1.09-2.19	0.015	1.51	1.05-2.19	0.028
Age	0.99	0.98-1.01	0.32			
Gender	0.7	0.46-1.07	0.097			
Histological	1.63	0.43-6.19	0.471			
Surgery	1.03	0.87-1.23	0.716			
T Stage	1.52	1.22-1.89	< 0.001	1.5	0.69-3.3	0.309
N Stage	1.19	0.29-4.88	0.808			
M Stage	2.42	0.59-9.9	0.219			
AJCC Grade	1.49	1.17-1.91	0.001	0.96	0.42-2.19	0.92

cant confounding bias from the small sample size of these stages. In T1-stage HCC patients, a significant correlation between acetyl-α-tubulin-lys40 level and prognosis was observed (**Figure 1B**). However, no significant difference was detected in the survival analysis of T2-stage HCC patients, possibly due to limited hypoacetylation cases (Supplementary Figure 1A). Our further stratified survival analysis revealed a poorer prognosis for patients with higher levels of acetyl-α-tubulin-lys40 in the early stages (T1 and T2) of HCC (Supplementary Figure 1B), but acetyl-α-tubulin-lys40 level did not impact the prognosis of advanced (T3 and T4) HCC patients (Supplementary Figure 1C). This provides a further demonstration of the prognostic ability of acetyl-α-tubulin-lys40 level in HCC patients, especially in early-stage HCC.

We constructed a prognostic prediction model using publicly available databases that incorporated various patient parameters, including age, gender, tumor stage, follow-up period, and acetyl-α-tubulin-lys40 level. Initially, our univariate Cox regression analysis revealed that acetyl-α-tubulin-lys40 level and tumor stage were significant prognostic indicators for the overall survival of HCC patients (**Table 1**). Subsequently, we performed multivariate Cox regression analysis on these two indicators, along with our previously identified risk factor, and confirmed that the level of acetyl-α-tubulin-lys40 was an independent risk factor for patient survival and prognosis (**Table 1**; **Figure 1C**). Consequently, we developed a nomogram to predict the overall survival of HCC patients, achieving a concordance index of 0.63 (**Figure 1D**).

High level of acetyl-α-tubulin-lys40 is correlated with poor prognosis in clinical data

We collected information and surgical pathological samples from HCC patients at Dongyang People's Hospital between September 2014 and September 2020. After thorough follow-up and screening procedures, 59 clinical surgical pathological samples from HCC patients were utilized to develop tissue microarrays (TMAs). Immunohistochemical staining and interpretation were performed on the TMAs, which included patient tumor specimens, paracancerous specimens, and normal tissue control specimens. Patient survival was monitored until January 31, 2023. Supplementary Table 2 displays the clinical characteristics of the patients included in our study. Immunohistochemical staining (IHC) of acetyl-α-tubulin-lys40 on pathological specimens using TMAs revealed higher levels in tumor tissues compared to adjacent non-tumor control tissues (**Figure 2A** and **2B**).

We utilized univariate Cox regression analysis to analyze survival differences across various factors including gender, age, T stage (clinical stage and T stage were considered consistent since both N stage and M stage were 0), acetyl-α-tubulin-lys40 level (categorized by the cutoff of 2), and histological grade (Supplementary Table 3); all factors showed no significant difference in OS. In the OS prognosis analysis, patients in the acetyl-α-tubulin-lys40 low-level group exhibited a relatively better survival prognosis than those in the high-level group (Supplementary Figure 2). Further stratified survival analysis revealed significantly better survival prognosis in stage T1 patients from

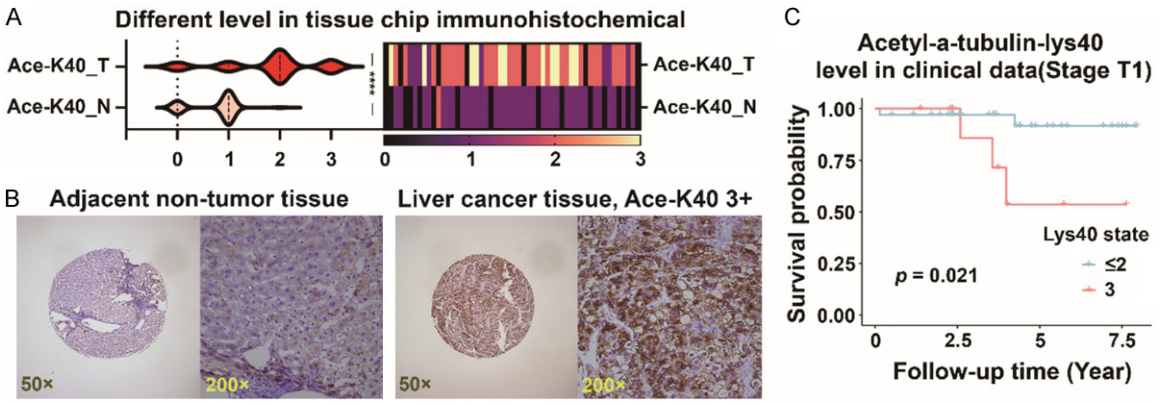

Figure 2. The level of acetyl-α-tubulin-lys40 was higher in liver tumors, correlated with poor prognosis in clinical data. A. The distribution of levels of acetyl-α-tubulin-lys40. The left part of the figure shows violin plots of protein distribution and the right part shows heat maps of protein levels (Legend: Ace-K40_T: level of acetyl-α-tubulin-lys40 in tumor tissue, Ace-K40_N: level of acetyl-α-tubulin-lys40 in adjacent non-tumor tissue, the x-axis of the violin plots represents the acetyl-α-tubulin-lys40 level, while the x-axis of the heat maps represents each sample from different cases, except for two lost samples. A total of 56 cases are included in the analysis, with different colors indicating different levels of acetyl-α-tubulin-lys40, specifically 0: black, 1: purple, 2: orange, 3: light yellow); B. Example of acetyl-α-tubulin-lys40 immunohistochemical staining results on tissue microarray (TMA) (50 × and 200 × magnification for each group); C. The OS analysis. The group with acetyl-α-tubulin-lys40 level ≤ 2 was classified as the low-level group, while the group with acetyl-α-tubulin-lys40 level = 3 was classified as the high-level group. The *p*-value was 0.021.

the low-level group (**Figure 2C**), indicating that acetyl-α-tubulin-lys40 level serves as a predictor for overall survival, particularly in early-stage HCC, T1 stage.

High level of acetyl-α-tubulin-lys40 is corelated with lower sensitivity to Eribulin in HCC cell lines

In clinical practice, anti-microtubule depolymerization drugs like paclitaxel are not considered front-line chemotherapy regimens due to their clinical trial failures [12, 67]. Eribulin, an anti-microtubule polymerization drug, inhibits tubulin polymerization and pharmacologically differs from paclitaxel. Therefore, we conducted a comparative experiment on paclitaxel and Eribulin in HCC cell lines. Results indicate that both HCCLM3 and Li-7 cell lines exhibit higher sensitivity to Eribulin than to paclitaxel (Supplementary Figure 3A), leading us to consider Eribulin's potential in HCC treatment over traditional anti-microtubule drugs like paclitaxel.

Prior research has suggested that α-tubulin acetylation enhances tubulin stability [64]. Consequently, we postulated that Eribulin might exhibit varied therapeutic effects on cells with different α-tubulin acetylation levels. Initially, we assessed acetyl-α-tubulin-lys40 levels across various unselected HCC cell lines, discovering variability in acetyl-α-tubulin-lys40 levels across different HCC cell lines (**Figure 3A**). We questioned whether cell lines demonstrate different sensitivities to Eribulin treatment based on their respective acetyl-α-tubulin-lys40 levels. After treating HCC cells with Eribulin and using the CCK-8 method to evaluate cell viability, we found that distinct HCC cell lines possess varied sensitivities to Eribulin (**Figure 3B**). Specifically, higher acetyl-α-tubulin-lys40 levels correlated with lower sensitivity to Eribulin treatment (**Figure 3B**). Thus, we theorize that HCC cell lines with elevated levels of acetyl-α-tubulin-lys40 are less sensitive to Eribulin treatment (**Figure 3A** and **3B**).

Subsequently, we categorized the HCC cell lines into three groups based on their sensitivity to Eribulin: resistant, moderately resistant, and sensitive (**Figure 3B**). To validate our hypothesis, we selected representative cell lines from each group for further testing. Results from CCK-8 and drug-sensitivity crystal violet staining revealed that cell lines with higher acetyl-α-tubulin-lys40 levels had higher via-

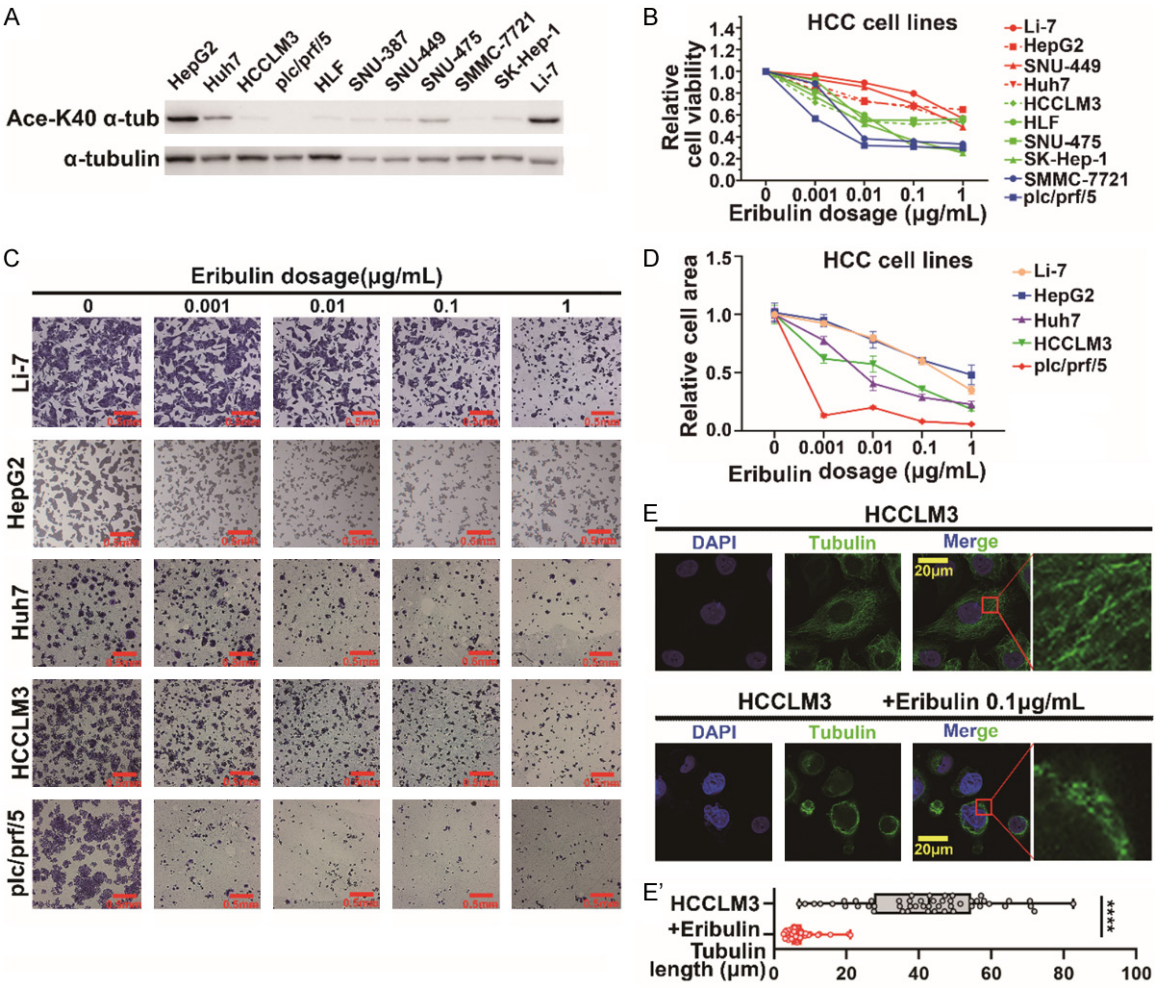

Figure 3. High level of acetyl-α-tubulin-lys40 corelated with lower sensitivity to Eribulin in HCC cell lines. (A) Different HCC cell lines exhibited differential levels of acetyl-α-tubulin-lys40; (B) Sensitivity analysis by CCK-8 of different HCC cells to Eribulin treatment at gradient concentration of 0~1 μg/mL; According to the relative cell viability at Eribulin concentrations of 0.001~0.01 μg/mL, the cell lines were classified into three groups with different sensitivities: resistant (red), moderate resistant (green), and sensitive (blue); (C) Sensitivity analysis of different HCC cells to Eribulin treatment at gradient concentrations of 0~1 μg/mL. Validation was carried out using crystal violet drug sensitivity experiments; (D) Visualizations of (C); (E) Visualization of immunofluorescence staining shown the different structure of microtubules between negative control and Eribulin treatment; (E') Statistics of tubulin length in (E) (measuring for 50 microtubules of each group).

bility under the same Eribulin concentration (**Figure 3C** and **3D**). This reaffirmed our earlier observation that acetyl-α-tubulin-lys40 levels are inversely related to Eribulin sensitivity.

To investigate differences in apoptosis among these cell lines, we employed flow cytometry and observed that apoptosis levels in plc/prf/5 cells were significantly elevated compared to other resistant lines (Supplementary Figure 3B and 3C). Based on these findings, we concluded that cells with low levels of acetyl-α-tubulin-lys40 were more vulnerable to Eribulin-induced apoptosis.

Prior studies have indicated that while Eribulin affects microtubule assembly, its impact differs from taxanes. To understand Eribulin's influence on microtubule morphology, we treated HCCLM3 cells with Eribulin (0.1 μg/mL for 48 hours) and performed immunofluorescence staining (**Figure 3E** and **3E'**). Eribulin treatment appeared to disrupt microtubule assembly, leading to discontinuous, scattered, and loose structures. To further investigate the role of Eribulin in microtubule polymerization, we conducted a semi-quantitative analysis of microtubule polymerization (Supplementary Figure 3D). We found that, in contrast to pacli-

taxel, Eribulin interfered with microtubule assembly in a dose-dependent manner.

Based on our previous results, which discovered a negative correlation between acetyl-α-tubulin-lys40 levels in HCC cells and their sensitivity to Eribulin, we speculated whether reducing acetyl-α-tubulin-lys40 levels in HCC cells might enhance Eribulin's therapeutic efficacy.

Reducing the level of acetyl-α-tubulin-lys40 could disturb the stability of microtubules

Previous studies have shown [59-62, 68] that Histone Deacetylase 6 (HDAC6) and Alpha Tubulin Acetyltransferase 1 (ATAT1) are key deacetylases and acetyltransferases, respectively, regulating acetylation levels of lysine 40 on α-tubulin (acetyl-α-tubulin-lys40) (**Figure 4A**). We further downloaded RNA expression data and associated clinical information for 365 LIHC tumor samples from TCGA, and performed an OS curve analysis on the HDAC6 and ATAT1 datasets without filtering. Results revealed that elevated HDAC6 expression and reduced ATAT1 expression correlated with improved overall survival (Supplementary Figure 4A and 4B). Given that elevated HDAC6 and reduced ATAT1 expression both suggest diminished acetyl-α-tubulin-lys40 levels, we further probed the relationship between acetyl-α-tubulin-lys40 and HCC patient OS. In our clinical surgical pathological samples, we conducted immunohistochemical staining for both ATAT1 and HDAC6 using TMAs (Supplementary Figure 4C). We observed a significantly higher level of ATAT1 in tumor tissues compared to adjacent non-tumor tissue, with no discernible difference in HDAC6 levels (**Figure 4B**). Given that elevated acetyl-α-tubulin-lys40 levels enhance microtubule stability, we performed immunofluorescence staining to examine tubulin morphology after knocking down ATAT1 and overexpressing HDAC6 in different HCC cells (**Figures 4C-E** and **4C'-E'**, **5A**, **5E**, **5I**, **6A**, **6E**, **6I**). We observed that in negative control cells, tubulin primarily exhibited a continuous linear structure with few punctate structures. However, in ATAT1 knockdown cells, tubulin was mostly distributed as scattered dots, with minimal visible cord-like microtubules. Overexpressing HDAC6 produced results consistent with ATAT1 knockdown findings (**Figure 4F-H** and **4F'-H'**). Thus, we inferred that reducing acetyl-α-tubulin-lys40 levels may impact tubulin assembly or microtubule stability.

Knockdown of ATAT1 reduces acetyl-α-tubulin-lys40 and sensitizes HCC cells to eribulin treatment

As previously mentioned, acetyltransferase ATAT1 mediates the acetylation of α-tubulin (**Figure 4A**). Given the influence of endogenous levels of acetyl-α-tubulin-lys40 on sensitivity to Eribulin (**Figure 3**), we examined if ATAT1-knockdown (ATAT1-KD) could improve Eribulin's efficacy. We knocked down ATAT1 in HCC cell lines such as Li-7, HCCLM3, and Hepa1-6, observing a reduction in acetyl-α-tubulin-lys40 levels (**Figure 5A**, **5E**, **5I**). We then assessed the Eribulin sensitivity of these HCC cell lines and found that ATAT1-KD as associated with increased viability loss induced by Eribulin (**Figure 5B-D**, **5F-H**, **5J-L**). Based on these experimental results, we concluded that diminishing ATAT1 levels in HCC cells effectively reduces acetyl-α-tubulin-lys40 levels, heightening the responsiveness of HCC cells to Eribulin treatment. Further tests on cell cycle and apoptosis revealed that Eribulin induced G2/M arrest and apoptosis more effectively in ATAT1-KD cells (Supplementary Figure 5A-F). Moreover, higher Eribulin concentrations had were associated with a more pronounced effect. Based on these findings, we conclude that ATAT1-KD can reduce acetyl-α-tubulin-lys40 levels, further enhancing the therapeutic efficacy of Eribulin in HCC cells via cell cycle arrest and apoptosis.

Overexpression of HDAC6 reduces acetylation level of acetyl-α-tubulin-lys40 and sensitizes HCC cells to eribulin treatment

Conversely, HDAC6 is known to remove α-tubulin acetylation (**Figure 4A**). Therefore, we also studied the effects of exogenous HDAC6 overexpression (HDAC6-OE) on Eribulin sensitivity in HCCLM3, Li-7, and Hepa1-6 cell lines. As anticipated, HDAC6-OE decreased the level of acetyl-α-tubulin-lys40 (**Figure 6A**, **6E**, **6I**) and enhanced Eribulin's efficacy, as indicated by reduced cell viability (**Figure 6B-D**, **6F-H**, **6J-L**). We concluded that HDAC6-OE can diminish acetyl-α-tubulin-lys40 levels in HCC cells, thereby boosting the sensitivity of these cells to Eribulin treatment. We also explored the influ-

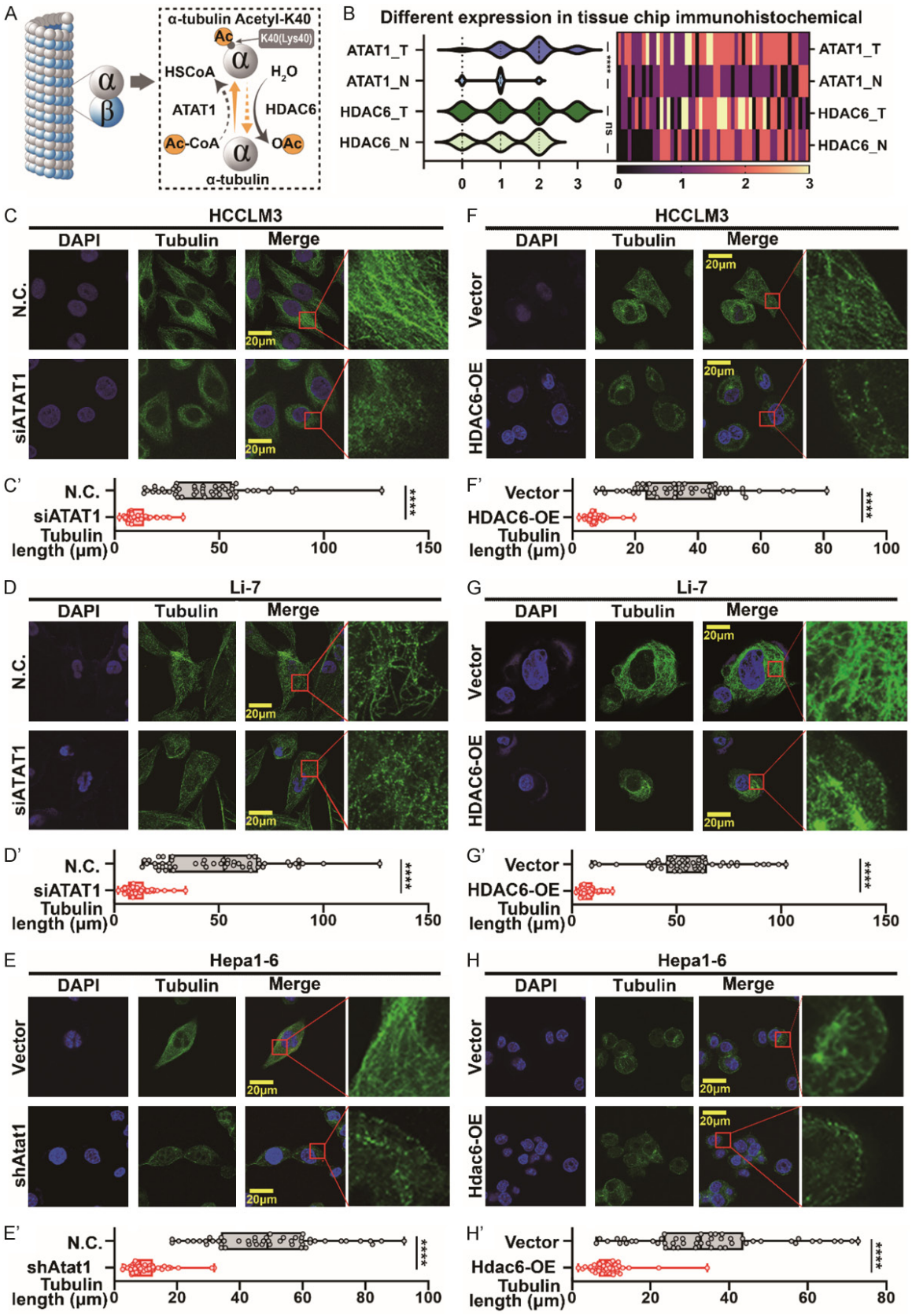

Figure 4. Reducing the level of acetyl-α-tubulin-lys40 could disturb the stability of microtubules. A. The left panel shows a schematic diagram of microtubules structure composed of a series of α-tubulin and β-tubulin subunits. Acetyl-a-tubulin-lys40 is a modification present at the 40th site of α-tubulin, which can be regulated by ATAT1 and

HDAC6 enzymes to maintain a dynamic balance of acetylation level; B. The distribution of protein expression levels of ATAT1 and HDAC6. The left part of the figure shows violin plots of expression distribution and the right part shows heat maps of protein expression levels (Legend: ATAT1_T: expression level of ATAT1 in tumor tissue, ATAT1_N: expression level of ATAT1 in adjacent non-tumor tissue, HDAC6_T: expression level of HDAC6 in tumor tissue, HDAC6_N: expression level of HDAC6 in adjacent non-tumor tissue, the x-axis of the violin plots represents the protein expression level, while the x-axis of the heat maps represents each sample from different cases, except for two lost samples. A total of 56 cases are included in the analysis, with different colors indicating different levels of protein expression, specifically 0: black, 1: purple, 2: orange, 3: light yellow); C-E. Knocking down ATAT1 in HCC cell lines, the microtubule shapes were observed and photographed under immunofluorescence microscopy (60 × oil objective lens) by staining cell nuclei with blue (DAPI) and tubulin with green. The merged images showed two different forms of microtubules: linear microtubules (with cavity and strip-like shape) and punctate microtubules (short, free microtubule fragments); C'-E'. Statistics of tubulin length in each group (measuring for 50 microtubules); C. Knocking down ATAT1 in HCCLM3; D. Knocking down ATAT1 in Li-7; E. Knocking down Atat1 in Hepa1-6; F-H. Overexpressing HDAC6 in HCC cell lines, the microtubule shapes were observed and photographed under immunofluorescence microscopy (60 × oil objective lens) by staining cell nuclei with blue (DAPI) and tubulin with green; F'-H'. Statistics of tubulin length in each group (measuring for 50 microtubules); F. Overexpressing HDAC6 in HCCLM3; G. Overexpressing HDAC6 in Li-7; H. Overexpressing Hdac6 in Hepa1-6.

ence of HDAC6 overexpression on cell cycle and apoptosis in HCC cells. The results paralleled those observed with ATAT1 knockdown (Supplementary Figure 6A-F). We observed an increase in G2/M phase arrest in HCCLM3 and Hepa1-6 Hdac6-OE cells, although no definitive trend was discerned in Li-7 cells. Quantification of apoptosis following treatment revealed that Eribulin led to an increased rate of apoptosis in HDAC6-OE HCC cells, particularly in early and late apoptosis stages. These outcomes suggest that HDAC6-OE reduces acetyl-α-tubulin-lys40 levels thereby potentiating the therapeutic efficacy of Eribulin.

Reduction of acetyl-α-tubulin-lys40 increases the sensitivity to Eribulin of HCC xenograft mice

In previous *in vitro* experiments, we confirmed that either ATAT1-KD or HDAC6-OE can reduce the level of acetyl-α-tubulin-lys40, thereby sensitizing cells to Eribulin treatment. To investigate if these results translated *in vivo*, we established a mouse tumor cell transplantation model by subcutaneously transplanting engineered Atat1-KD or Hdac6-OE Hepa1-6 cells to C57BL/6 mice (Supplementary Figure 7A). We then conducted statistical analyses on the size of formed subcutaneous tumors. In mice implanted with Atat1-KD cells, the tumors in the treatment group were significantly smaller than those in the control group. Analysis using the χ^2 (and Fisher's exact) test showed a significant trend, wherein tumors in Atat1-KD Eribulin-treated mice were the smallest among all groups starting from day 7 (**Figure 7A**). At the study's conclusion, we compared tumor sizes and tumor weight using the χ^2 (and Fisher's exact) test (**Figure 7B-D**); tumors from Atat1-KD Eribulin-treated mice were found to be the lightest.

In the Hdac6-OE tumor cell transplantation model, the growth rate of tumors with Hdac6-OE cells treated with Eribulin was the slowest, with a significant difference observed amongst all groups from day 7 onward (**Figure 7F**). Further statistical analyses on tumor weight at the end of the experiment revealed a similar trend (**Figure 7G-I**). Immunohistochemistry results (**Figure 7E** and **7J**) showed that knocking down Atat1 or overexpressing Hdac6 decreased the levels of acetyl-α-tubulin-lys40 (Ace-K40). Additionally, Ki-67 expression in Eribulin-treated groups with low Ace-K40 levels was lower than in those with high Ace-K40 levels, indicating a reduced proliferation rate. These findings demonstrate that lowering acetyl-α-tubulin-lys40 levels in tumor cells can enhance their sensitivity to Eribulin treatment *in vivo*.

Eribulin has demonstrated considerable safety in preclinical experiments and clinical trials [19-22]. Throughout our study, we monitored changes in mouse body weight during treatment (Supplementary Figure 7B and 7C). We observed that, whether in the Atat1 knockdown or Hdac6 overexpression groups, there was no significant difference in body weight compared to the negative control group. This suggests that Eribulin treatment at the administered concentration did not exhibit noticeable toxicity.

Discussion

Microtubule-targeted drugs have become a focal point in anti-tumor chemotherapy. As new anti-microtubule drugs continue to be devel-

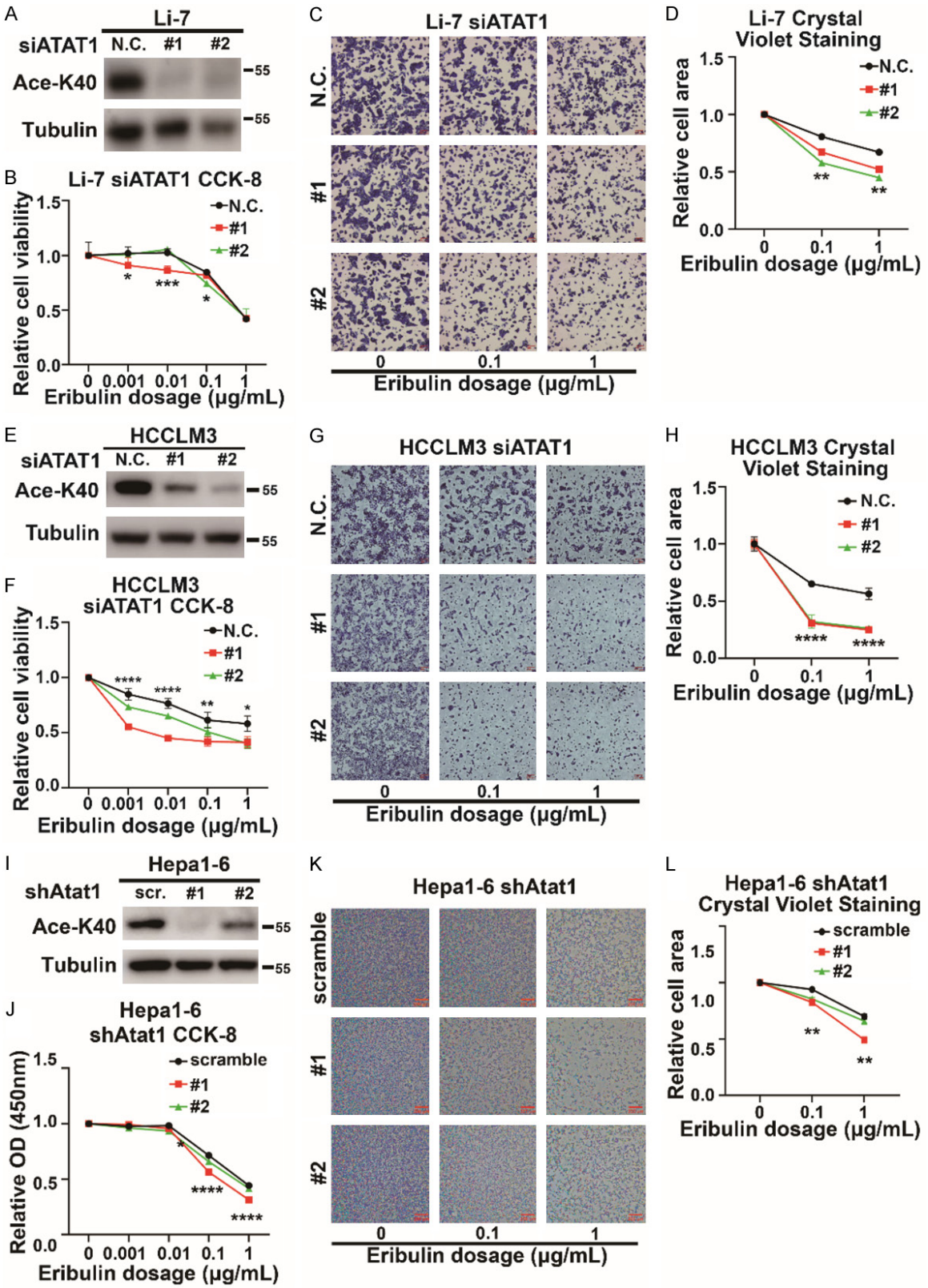

Figure 5. Loss of ATAT1 could increase the sensitivity to Eribulin of HCC cells. A-D. Knockdown of ATAT1 in human HCC cell line Li-7 by transient transfection with siATAT1 construct increased the sensitivity of HCC cells to Eribulin treatment; A. Level changes of acetyl-α-tubulin-lys40 in Li-7 cells after knockdown of ATAT1; B. Detection of changes in sensitivity of ATAT1-knockdown Li-7 cells to Eribulin treatment using the CCK-8 assay; C. Microscopic observation of crystal violet drug sensitivity experiments in ATAT1-knockdown Li-7 cells; D. Visualization of data of crystal violet

drug sensitivity experiments in ATAT1-knockdown Li-7 cells; E-H. Knockdown of ATAT1 in human HCC cell line HCCLM3 by transient transfection with siATAT1 construct increased the sensitivity of HCC cells to Eribulin treatment; E. Level changes of acetyl-α-tubulin-lys40 in HCCLM3 cells after knockdown of ATAT1; F. Detection of changes in sensitivity of ATAT1-knockdown HCCLM3 cells to Eribulin treatment using the CCK-8 assay; G. Microscopic observation of crystal violet drug sensitivity experiments in ATAT1-knockdown HCCLM3 cells; H. Visualization of data of crystal violet drug sensitivity experiments in ATAT1-knockdown HCCLM3 cells; I-L. Knockdown of Atat1 in mouse HCC cell line Hepa1-6 by stable transfection with shRNA construct increased the sensitivity of cells to Eribulin treatment; I. Level changes of acetyl-α-tubulin-lys40 in Hepa1-6 cells after knockdown of Atat1; J. Detection of changes in sensitivity of Atat1-knockdown Hepa1-6 cells to Eribulin treatment using the CCK-8 assay; K. Microscopic observation of crystal violet drug sensitivity experiments in Atat1-knockdown Hepa1-6 cells; L. Visualization of data of crystal violet drug sensitivity experiments in Atat1-knockdown Hepa1-6 cells.

oped, a significant portion of current research is dedicated to understanding drug resistance mechanisms. Consequently, reversing drug resistance has emerged as a crucial research direction. Our study began with the aim to identify populations sensitive to Eribulin treatment and to understand the impact of the 40th-site-lysine acetylation level of α-tubulin on drug sensitivity. We discovered that the acetyl-α-tubulin-lys40 level serves as both a survival and prognosis indicator in HCC, and also as a marker for Eribulin treatment sensitivity. Specifically, a reduction in acetyl-α-tubulin-lys40 enhances tumor sensitivity to Eribulin. This finding has potential guiding significance for clinical treatment.

Based on the statistical analysis of HCC patient data in the public database, we found a significant negative correlation between the level of acetyl-α-tubulin-lys40 and HCC patient prognosis. Subsequent data analysis indicated that the acetyl-α-tubulin-lys40 level is an independent risk factor for survival and prognosis in HCC patients. We further established a prognostic assessment nomogram after screening the corresponding data. However, since the interpretation of acetyl-α-tubulin-lys40 in clinical samples cannot be aligned with the protein RPPA data in TCPA database, it is impossible to use these data for external verification of the nomogram, which is a shortcoming of this study.

We collected pathological specimens from HCC patients in our center and conducted long-term follow-ups, constructed TMAs of the pathological specimens, and performed IHC on acetyl-α-tubulin-lys40, ATAT1 and HDAC6. We observed that the survival curves of patients with low levels of acetyl-α-tubulin-lys40 and those with high levels did not yield statistically significant results. However, the survival curves separated from each other, revealing that high-level group patients had a worse trend of survival. In comparison with the public database, we were unsuccessful in obtaining similar results in our comprehensive HCC patient data analysis. Potential reasons include a short follow-up duration, fewer patients in the high-level group, most follow-up patients being at stage I, based on TNM staging, which may cause a substantial admission rate bias, and the limited scale of our clinical cohort. However, we can expand the sample size or collect cases from multiple centers. Furthermore, by quantifying the acetyl-α-tubulin-lys40 score in patient pathological specimens, patients with high and low acetyl-α-tubulin-lys40 levels would be more accurately distinguished by calculating the cutoff value.

Although Eribulin has been used in clinical practice for more than three years since its introduction to China, the number of patients who have received this treatment remains limited. This scarcity of patients makes it challenging to obtain comprehensive data from either clinical practices or databases. Additionally, further research is essential to clarify the relationship between changes in acetyl-α-tubulin-lys40 levels before and after Eribulin treatment with its therapeutic efficacy.

In clinical practice, selective HDAC inhibitors, such as Vorinostat, Romidepsin, Belinostat, Panobinostat, Entinostat, and Epidaza, are employed to treat lymphoma and breast cancer. The HDAC family comprises four classes containing 18 types of HDACs [69]. Selective HDAC inhibitors typically target various HDACs; for example, Epidaza targets HDAC1, 2, 3, 10, while Vorinostat targets HDAC1, 2, 3, 5, 6, 8, 9, 10, 11. When targeting HDACs, the activity of selective HDAC inhibitors reduces histone acetylation, leading to the compaction of the

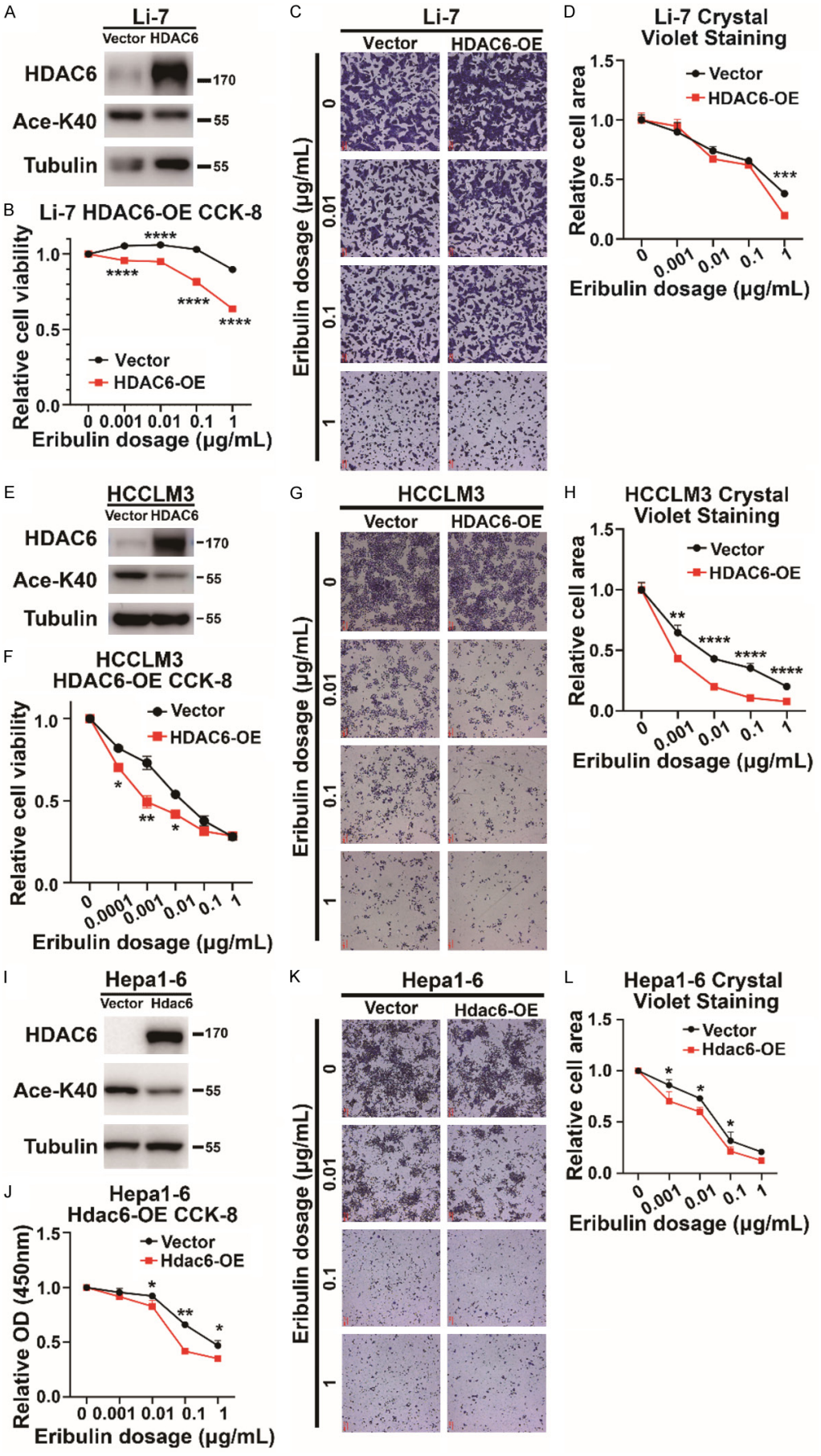
A
Li-7
Vector HDAC6
HDAC6
Ace-K40
Tubulin
170
55
55
B
Li-7 HDAC6-OE CCK-8
Relative cell viability
Vector
HDAC6-OE
Eribulin dosage (μg/mL)
C
Li-7
Vector
HDAC6-OE
Eribulin dosage (μg/mL)
D
Li-7 Crystal Violet Staining
Relative cell area
Vector
HDAC6-OE
Eribulin dosage (μg/mL)
E
HCCLM3
Vector HDAC6
HDAC6
Ace-K40
Tubulin
F
HCCLM3 HDAC6-OE CCK-8
Relative cell viability
G
HCCLM3
H
HCCLM3 Crystal Violet Staining
I
Hepa1-6
Vector Hdac6
J
Hepa1-6 Hdac6-OE CCK-8
Relative OD (450nm)
K
Hepa1-6
Vector
Hdac6-OE
L
Hepa1-6 Crystal Violet Staining

Figure 6. HDAC overexpression could increase the sensitivity to Eribulin in HCC cells. A-D. Overexpressing HDAC6 in Li-7 by stable transfection increased the sensitivity of cells to Eribulin treatment; A. Level changes of acetyl-α-tubulin-lys40 in Li-7 cells after overexpressing HDAC6; B. Detection of changes in sensitivity of HDAC-OE Li-7 cells to Eribulin treatment using the CCK-8 assay; C. Microscopic observation of crystal violet drug sensitivity experiments in HDAC6-OE Li-7 cells; D. Visualization of data of crystal violet drug sensitivity experiments in HDAC6-OE Li-7 cells; E-H. Overexpressing HDAC6 in HCCLM3 by stable transfection increased the sensitivity of cells to Eribulin treatment; E. Level changes of acetyl-α-tubulin-lys40 in HCCLM3 cells after overexpressing HDAC6; F. Detection of changes in sensitivity of HDAC-OE HCCLM3 cells to Eribulin treatment using the CCK-8 assay; G. Microscopic observation of crystal violet drug sensitivity experiments in HDAC6-OE HCCLM3 cells; H. Visualization of data of crystal violet drug sensitivity experiments in HDAC6-OE HCCLM3 cells; I-L. Overexpressing Hdac6 in Hepa1-6 by stable transfection increased the sensitivity of cells to Eribulin treatment; I. Level changes of acetyl-α-tubulin-lys40 in Hepa1-6 cells after overexpressing Hdac6; J. Detection of changes in sensitivity of Hdac6-OE Hepa1-6 cells to Eribulin treatment using the CCK-8 assay; K. Microscopic observation of crystal violet drug sensitivity experiments in Hdac6-OE Hepa1-6 cells; L. Visualization of data of crystal violet drug sensitivity experiments in Hdac6-OE Hepa1-6 cells.

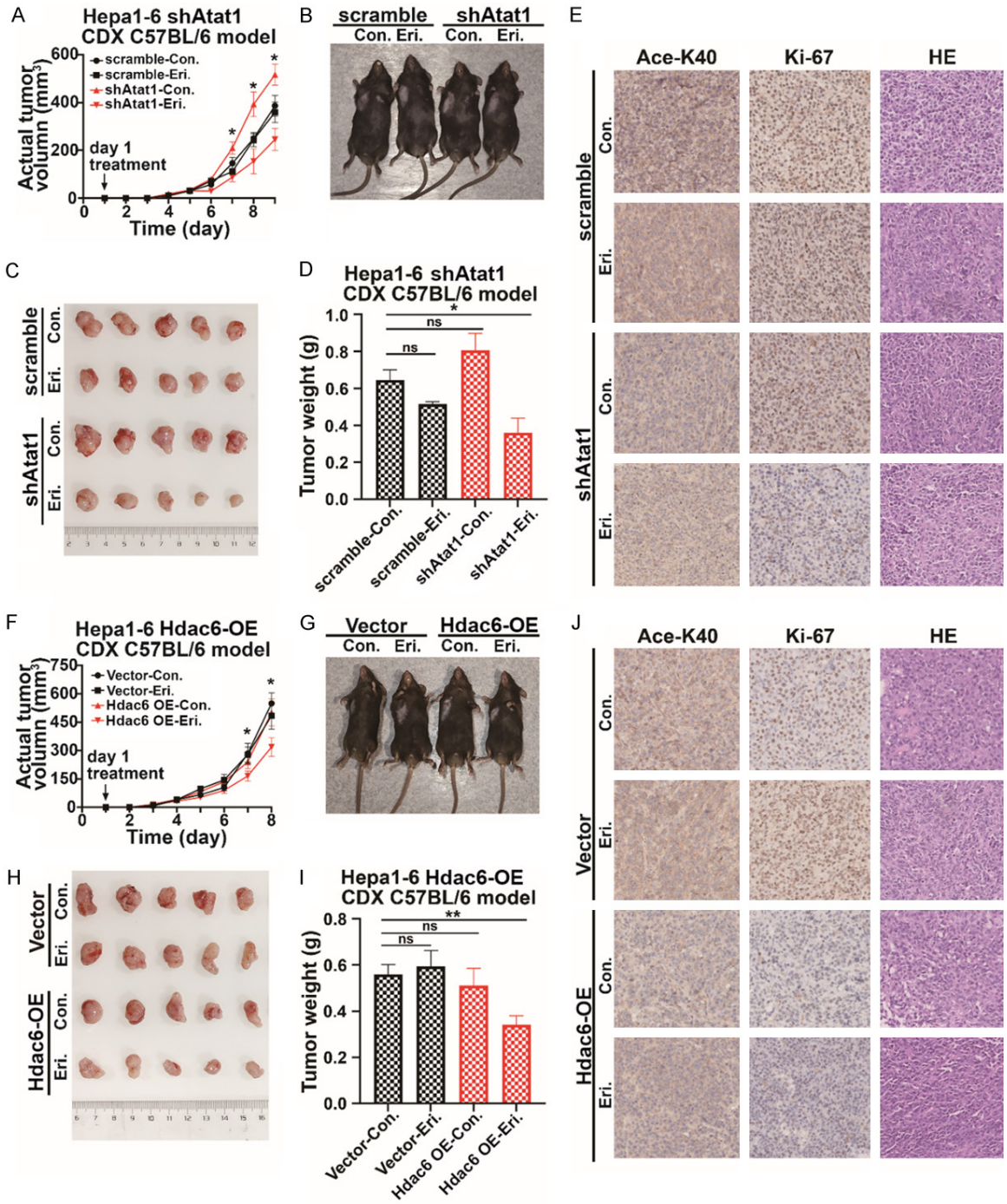

Figure 7. Loss of ATAT1 or HDAC6 overexpression could increase the treatment effect of Eribulin *in vivo*. (A) Knockdown of Atat1 in Hepa1-6 cells for cell tumor transplantation model in C57BL/6 mice. Administration started on day 1, and tumor size change curve was observed; (B) Macroscopic photo of transplanted tumors in mice before dissection; (C) Macroscopic observation of transplanted tumors in dissected mice; (D) Final tumor weight of experimental mice with Atat1 knockdown; (E) The immunohistochemistry results of the tumors in (C), stained with Ace-K40, Ki-67 and HE (hematoxylin-eosin); (F) Overexpression of Hdac6 in Hepa1-6 cells for tumor transplantation model in C57BL/6 mice. Administration started on day 1, and tumor size change curve was observed; (G) Macroscopic photo of transplanted tumors in mice before dissection; (H) Macroscopic observation of transplanted tumors in dissected mice; (I) Final tumor weight of experimental mice with Hdac6 overexpression; (J) The immunohistochemistry results of the tumors in (H), stained with Ace-K40, Ki-67 and HE (hematoxylin-eosin).

DNA/histone complex. This compaction further promotes growth arrest, differentiation, and apoptosis of tumor cells [70]. Previous studies have predominantly focused on the chromatin histone acetylation of HDAC inhibitors. Fewer studies have concentrated on HDAC6, which can also regulate the acetylation of microtubules. Our research revealed that overexpressing HDAC6 can decrease the acetyl-α-tubulin-lys40 level, impacting the assembly process of microtubules, and thereby enhancing the therapeutic efficacy of Eribulin.

In this study, we focused on investigating the impact of acetyl-α-tubulin-lys40 levels on the prognosis of HCC patients. Our findings suggest that decreasing the acetyl-α-tubulin-lys40 level can augment Eribulin-induced cell cycle arrest and apoptosis, especially in cells with elevated acetyl-α-tubulin-lys40 levels. This reduction also enhances sensitivity to Eribulin treatment. Moreover, in our *in vivo* experiments, Eribulin treatment was more effective in tumors with reduced acetyl-α-tubulin-lys40 levels, evident in both ATAT1-KD and HDAC6-OE groups. Since our model utilized a murine cell line, additional *in vivo* studies using human HCC cell lines are warranted. Given these insights, our goal was to determine if diminishing the acetylation level could render patients more receptive to Eribulin treatment, amplifying the benefits especially for those with elevated acetyl-α-tubulin-lys40 levels. We started screening potential drugs on CellMiner to achieve this aim but found no corresponding medicines. Subsequent literature searches on PubMed, however, and found some existing medicines in clinical practice, such as estradiol, tamoxifen, and metformin, which can reduce the level of acetyl-α-tubulin-lys40 by increasing the expression level of HDAC6. Notably, these drugs have good safety profiles in clinical application. Preliminary investigations revealed their distinct influence on the protein expression levels of HDAC6 [71-75]. However, the effective concentration and mechanism of action are still being explored. We hope to continue exploring these drug candidates to achieve the goal of sensitizing Eribulin treatment through the new application of these known drugs. If we identify a capable of reducing the level of acetyl-α-tubulin-lys40 and sensitize Eribulin treatment, it may lay the foundation for a wider application of Eribulin, as currently its treatment indications are limited to advanced breast cancer and liposarcoma. Our research may pave the way for further experimental exploration and clinical practice in the future, particularly for expanding the use of Eribulin in patients with low acetyl-α-tubulin-lys40 levels.

Conclusion

Our findings indicate that lowering acetyl-α-tubulin-lys40 levels in HCC can amplify the therapeutic efficacy of Eribulin, both *in vitro* and *in vivo*. Furthermore, we demonstrate that acetyl-α-tubulin-lys40 could be a potential prognostic marker and predictive indicator for Eribulin treatment benefit in HCC patients.

Acknowledgements

This work was supported by the National Natural Science Foundation of China (32000519) and the Natural Science Foundation of Zhejiang Province, China (LQ21C080001).

Disclosure of conflict of interest

None.

Address correspondence to: Dr. Jia Zhou and Hongchuan Jin, Laboratory of Cancer Biology, Key Lab of Biotherapy in Zhejiang Province, Cancer Center of Zhejiang University, Sir Run Run Shaw Hospital, School of Medicine, Zhejiang University, Hangzhou 310016, Zhejiang, China. E-mail: zhoujia90@zju.edu.cn (JZ); jinhc@zju.edu.cn (HCJ)

References

[1] Sung H, Ferlay J, Siegel RL, Laversanne M, Soerjomataram I, Jemal A and Bray F. Global cancer statistics 2020: GLOBOCAN estimates of incidence and mortality worldwide for 36 cancers in 185 countries. CA Cancer J Clin 2021; 71: 209-249.

[2] Zheng R, Zhang S, Zeng H, Wang S, Sun K, Chen R, Li L, Wei W and He J. Cancer incidence and mortality in China, 2016. J Natl Cancer Cent 2022; 2: 1-9.

[3] Qing SK, Lu SC, Qiu WS, et al. China primary liver cancer clinical registry survey (CLCS) 2022 survival analysis update report. Congerence Name. 2022.

[4] Llovet JM, Burroughs A and Bruix J. Hepatocellular carcinoma. Lancet 2003; 362: 1907-1917.

[5] Liu CY, Chen KF and Chen PJ. Treatment of liver cancer. Cold Spring Harb Perspect Med 2015; 5: a021535.

[6] Llovet JM, Castet F, Heikenwalder M, Maini MK, Mazzaferro V, Pinato DJ, Pikarsky E, Zhu AX and Finn RS. Immunotherapies for hepatocellular carcinoma. Nat Rev Clin Oncol 2022; 19: 151-172.

[7] Llovet JM, Pinyol R, Kelley RK, El-Khoueiry A, Reeves HL, Wang XW, Gores GJ and Villanueva A. Molecular pathogenesis and systemic therapies for hepatocellular carcinoma. Nat Cancer 2022; 3: 386-401.

[8] Pinter M, Scheiner B and Pinato DJ. Immune checkpoint inhibitors in hepatocellular carcinoma: emerging challenges in clinical practice. Lancet Gastroenterol Hepatol 2023; 8: 760-770.

[9] Rimassa L, Finn RS and Sangro B. Combination immunotherapy for hepatocellular carcinoma. J Hepatol 2023; 79: 506-515.

[10] Liu Z, Lin Y, Zhang J, Zhang Y, Li Y, Liu Z, Li Q, Luo M, Liang R and Ye J. Molecular targeted and immune checkpoint therapy for advanced hepatocellular carcinoma. J Exp Clin Cancer Res 2019; 38: 447.

[11] Guo J, Zhao J, Xu Q and Huang D. Resistance of lenvatinib in hepatocellular carcinoma. Curr Cancer Drug Targets 2022; 22: 865-878.

[12] Chao Y, Chan WK, Birkhofer MJ, Hu OY, Wang SS, Huang YS, Liu M, Whang-Peng J, Chi KH, Lui WY and Lee SD. Phase II and pharmacokinetic study of paclitaxel therapy for unresectable hepatocellular carcinoma patients. Br J Cancer 1998; 78: 34-39.

[13] Anwanwan D, Singh SK, Singh S, Saikam V and Singh R. Challenges in liver cancer and possible treatment approaches. Biochim Biophys Acta Rev Cancer 2020; 1873: 188314.

[14] Llovet JM, Kelley RK, Villanueva A, Singal AG, Pikarsky E, Roayaie S, Lencioni R, Koike K, Zucman-Rossi J and Finn RS. Hepatocellular carcinoma. Nat Rev Dis Primers 2021; 7: 6.

[15] Demir T, Lee SS and Kaseb AO. Systemic therapy of liver cancer. Adv Cancer Res 2021; 149: 257-294.

[16] Hu A, Wei Z, Zheng Z, Luo B, Yi J, Zhou X and Zeng C. A computational framework to identify transcriptional and network differences between hepatocellular carcinoma and normal liver tissue and their applications in repositioning drugs. Biomed Res Int 2021; 2021: 9921195.

[17] Jain S and Vahdat LT. Eribulin mesylate. Clin Cancer Res 2011; 17: 6615-6622.

[18] Wilson K, de Rond T, Burkhardt I, Steele TS, Schafer RJB, Podell S, Allen EE and Moore BS. Terpene biosynthesis in marine sponge animals. Proc Natl Acad Sci U S A 2023; 120: e2220934120.

[19] Vahdat LT, Pruitt B, Fabian CJ, Rivera RR, Smith DA, Tan-Chiu E, Wright J, Tan AR, Dacosta NA, Chuang E, Smith J, O'Shaughnessy J, Shuster DE, Meneses NL, Chandrawansa K, Fang F, Cole PE, Ashworth S and Blum JL. Phase II study of eribulin mesylate, a halichondrin B analog, in patients with metastatic breast cancer previously treated with an anthracycline and a taxane. J Clin Oncol 2009; 27: 2954-2961.

[20] Goel S, Mita AC, Mita M, Rowinsky EK, Chu QS, Wong N, Desjardins C, Fang F, Jansen M, Shuster DE, Mani S and Takimoto CH. A phase I study of eribulin mesylate (E7389), a mechanistically novel inhibitor of microtubule dynamics, in patients with advanced solid malignancies. Clin Cancer Res 2009; 15: 4207-4212.

[21] Arnold SM, Moon J, Williamson SK, Atkins JN, Ou SH, LeBlanc M and Urba SG. Phase II evaluation of eribulin mesylate (E7389, NSC 707389) in patients with metastatic or recurrent squamous cell carcinoma of the head and neck: Southwest Oncology Group trial S0618. Invest New Drugs 2011; 29: 352-359.

[22] Cortes J, Vahdat L, Blum JL, Twelves C, Campone M, Roche H, Bachelot T, Awada A, Paridaens R, Goncalves A, Shuster DE, Wanders J, Fang F, Gurnani R, Richmond E, Cole PE, Ashworth S and Allison MA. Phase II study of the halichondrin B analog eribulin mesylate in patients with locally advanced or metastatic breast cancer previously treated with an anthracycline, a taxane, and capecitabine. J Clin Oncol 2010; 28: 3922-3928.

[23] Yuan P, Hu X, Sun T, Li W, Zhang Q, Cui S, Cheng Y, Ouyang Q, Wang X, Chen Z, Hiraiwa M, Saito K, Funasaka S and Xu B. Eribulin mesilate versus vinorelbine in women with locally

recurrent or metastatic breast cancer: a randomised clinical trial. Eur J Cancer 2019; 112: 57-65.
[24] Huyck TK, Gradishar W, Manuguid F and Kirkpatrick P. Eribulin mesylate. Nat Rev Drug Discov 2011; 10: 173-174.
[25] Mittal S, Kadamberi IP, Chang H, Wang F, Kumar S, Tsaih SW, Walker CJ, Chaluvally-Raghavan P, Charlson J, Landesman Y and Pradeep S. Preclinical activity of selinexor in combination with eribulin in uterine leiomyosarcoma. Exp Hematol Oncol 2023; 12: 78.
[26] Sachdev P, Ronen R, Dutkowski J and Littlefield BA. Systematic analysis of genetic and pathway determinants of Eribulin sensitivity across 100 human cancer cell lines from the cancer cell line encyclopedia (CCLE). Cancers (Basel) 2022; 14: 4532.
[27] Sato J, Shimizu T, Koyama T, Iwasa S, Shimomura A, Kondo S, Kitano S, Yonemori K, Fujiwara Y, Tamura K, Suzuki T, Takase T, Nagai R, Yamaguchi K, Semba T, Zhao ZM, Ren M and Yamamoto N. Dose escalation data from the phase 1 study of the liposomal formulation of Eribulin (E7389-LF) in Japanese patients with advanced solid tumors. Clin Cancer Res 2022; 28: 1783-1791.
[28] Shitara K, Hirao M, Iwasa S, Oshima T, Komatsu Y, Kawazoe A, Sato Y, Hamakawa T, Yonemori K, Machida N, Yuki S, Suzuki T, Okumura S, Takase T, Semba T, Zimmermann B, Teng A and Yamaguchi K. Phase I study of the liposomal formulation of Eribulin (E7389-LF): results from the advanced gastric cancer expansion cohort. Clin Cancer Res 2023; 29: 1460-1467.
[29] Vicari HP, Lima K, Costa-Lotufo LV and Machado-Neto JA. Cellular and molecular effects of Eribulin in preclinical models of hematologic neoplasms. Cancers (Basel) 2022; 14: 6080.
[30] Yoshihiro T, Ariyama H, Yamaguchi K, Imajima T, Yamaga S, Tsuchihashi K, Isobe T, Kusaba H, Akashi K and Baba E. Inhibition of insulin-like growth factor-1 receptor enhances eribulin-induced DNA damage in colorectal cancer. Cancer Sci 2022; 113: 4207-4218.
[31] Nisar A, Mamat AS, Hatim MI, Aslam MS and Syarhabil M. An updated review on Catharanthus roseus: phytochemical and pharmacological analysis. Indian Research Journal of Pharmacy and Science 2016; 3: 631-653.
[32] Virmani O, Srivastava G and Singh P. Catharanthus roseus--the tropical periwinkle. Indian Drugs 1978.
[33] Rowinsky EK, Cazenave LA and Donehower RC. Taxol: a novel investigational antimicrotubule agent. J Natl Cancer Inst 1990; 82: 1247-1259.
[34] Yamaguchi S, Maida Y, Yasukawa M, Kato T, Yoshida M and Masutomi K. Eribulin mesylate targets human telomerase reverse transcriptase in ovarian cancer cells. PLoS One 2014; 9: e112438.
[35] Towle MJ, Salvato KA, Budrow J, Wels BF, Kuznetsov G, Aalfs KK, Welsh S, Zheng W, Seletsky BM, Palme MH, Habgood GJ, Singer LA, Dipietro LV, Wang Y, Chen JJ, Quincy DA, Davis A, Yoshimatsu K, Kishi Y, Yu MJ and Littlefield BA. In vitro and in vivo anticancer activities of synthetic macrocyclic ketone analogues of halichondrin B. Cancer Res 2001; 61: 1013-1021.
[36] Jordan MA, Kamath K, Manna T, Okouneva T, Miller HP, Davis C, Littlefield BA and Wilson L. The primary antimitotic mechanism of action of the synthetic halichondrin E7389 is suppression of microtubule growth. Mol Cancer Ther 2005; 4: 1086-1095.
[37] Bai RL, Paull KD, Herald CL, Malspeis L, Pettit GR and Hamel E. Halichondrin B and homohalichondrin B, marine natural products binding in the vinca domain of tubulin. Discovery of tubulin-based mechanism of action by analysis of differential cytotoxicity data. J Biol Chem 1991; 266: 15882-15889.
[38] Kuznetsov G, Towle MJ, Cheng H, Kawamura T, TenDyke K, Liu D, Kishi Y, Yu MJ and Littlefield BA. Induction of morphological and biochemical apoptosis following prolonged mitotic blockage by halichondrin B macrocyclic ketone analog E7389. Cancer Res 2004; 64: 5760-5766.
[39] Gourmelon C, Frenel JS and Campone M. Eribulin mesylate for the treatment of late-stage breast cancer. Expert Opin Pharmacother 2011; 12: 2883-2890.
[40] Kaur R, Kaur G, Gill RK, Soni R and Bariwal J. Recent developments in tubulin polymerization inhibitors: an overview. Eur J Med Chem 2014; 87: 89-124.
[41] Gracheva IA, Shchegravina ES, Schmalz HG, Beletskaya IP and Fedorov AY. Colchicine alkaloids and synthetic analogues: current progress and perspectives. J Med Chem 2020; 63: 10618-10651.
[42] Jordan MA and Wilson L. Microtubules as a target for anticancer drugs. Nat Rev Cancer 2004; 4: 253-265.
[43] Naaz F, Haider MR, Shafi S and Yar MS. Anti-tubulin agents of natural origin: targeting taxol, vinca, and colchicine binding domains. Eur J Med Chem 2019; 171: 310-331.
[44] Perez-Perez MJ, Priego EM, Bueno O, Martins MS, Canela MD and Liekens S. Blocking blood flow to solid tumors by destabilizing tubulin: an approach to targeting tumor growth. J Med Chem 2016; 59: 8685-8711.

[45] Quail DF and Joyce JA. Microenvironmental regulation of tumor progression and metastasis. Nat Med 2013; 19: 1423-1437.
[46] Parker AL, Kavallaris M and McCarroll JA. Microtubules and their role in cellular stress in cancer. Front Oncol 2014; 4: 153.
[47] Haider K, Rahaman S, Yar MS and Kamal A. Tubulin inhibitors as novel anticancer agents: an overview on patents (2013-2018). Expert Opin Ther Pat 2019; 29: 623-641.
[48] Steinmetz MO and Prota AE. Microtubule-targeting agents: strategies to hijack the cytoskeleton. Trends Cell Biol 2018; 28: 776-792.
[49] Cui YJ, Liu C, Ma CC, Ji YT, Yao YL, Tang LQ, Zhang CM, Wu JD and Liu ZP. SAR investigation and discovery of water-soluble 1-methyl-1,4-dihydroindeno[1,2-c]pyrazoles as potent tubulin polymerization inhibitors. J Med Chem 2020; 63: 14840-14866.
[50] Prota AE, Bargsten K, Zurwerra D, Field JJ, Diaz JF, Altmann KH and Steinmetz MO. Molecular mechanism of action of microtubule-stabilizing anticancer agents. Science 2013; 339: 587-590.
[51] Seligmann J and Twelves C. Tubulin: an example of targeted chemotherapy. Future Med Chem 2013; 5: 339-352.
[52] Peris L, Thery M, Faure J, Saoudi Y, Lafanechere L, Chilton JK, Gordon-Weeks P, Galjart N, Bornens M, Wordeman L, Wehland J, Andrieux A and Job D. Tubulin tyrosination is a major factor affecting the recruitment of CAP-Gly proteins at microtubule plus ends. J Cell Biol 2006; 174: 839-849.
[53] Kubo T, Yanagisawa HA, Yagi T, Hirono M and Kamiya R. Tubulin polyglutamylation regulates axonemal motility by modulating activities of inner-arm dyneins. Curr Biol 2010; 20: 441-445.
[54] Magiera MM, Singh P, Gadadhar S and Janke C. Tubulin posttranslational modifications and emerging links to human disease. Cell 2018; 173: 1323-1327.
[55] Barisic M, Silva e Sousa R, Tripathy SK, Magiera MM, Zaytsev AV, Pereira AL, Janke C, Grishchuk EL and Maiato H. Mitosis. Microtubule detyrosination guides chromosomes during mitosis. Science 2015; 348: 799-803.
[56] L'Hernault SW and Rosenbaum JL. Chlamydomonas alpha-tubulin is posttranslationally modified in the flagella during flagellar assembly. J Cell Biol 1983; 97: 258-263.
[57] Sharom FJ. ABC multidrug transporters: structure, function and role in chemoresistance. Pharmacogenomics 2008; 9: 105-127.
[58] Allfrey VG, Faulkner R and Mirsky AE. Acetylation and methylation of histones and their possible role in the regulation of Rna synthesis. Proc Natl Acad Sci U S A 1964; 51: 786-794.
[59] Akella JS, Wloga D, Kim J, Starostina NG, Lyons-Abbott S, Morrissette NS, Dougan ST, Kipreos ET and Gaertig J. MEC-17 is an alpha-tubulin acetyltransferase. Nature 2010; 467: 218-222.
[60] Hubbert C, Guardiola A, Shao R, Kawaguchi Y, Ito A, Nixon A, Yoshida M, Wang XF and Yao TP. HDAC6 is a microtubule-associated deacetylase. Nature 2002; 417: 455-458.
[61] Zhang Y, Li N, Caron C, Matthias G, Hess D, Khochbin S and Matthias P. HDAC-6 interacts with and deacetylates tubulin and microtubules in vivo. EMBO J 2003; 22: 1168-1179.
[62] Matsuyama A, Shimazu T, Sumida Y, Saito A, Yoshimatsu Y, Seigneurin-Berny D, Osada H, Komatsu Y, Nishino N, Khochbin S, Horinouchi S and Yoshida M. In vivo destabilization of dynamic microtubules by HDAC6-mediated deacetylation. EMBO J 2002; 21: 6820-6831.
[63] Xu Z, Schaedel L, Portran D, Aguilar A, Gaillard J, Marinkovich MP, Thery M and Nachury MV. Microtubules acquire resistance from mechanical breakage through intralumenal acetylation. Science 2017; 356: 328-332.
[64] Li L, Wei D, Wang Q, Pan J, Liu R, Zhang X and Bao L. MEC-17 deficiency leads to reduced alpha-tubulin acetylation and impaired migration of cortical neurons. J Neurosci 2012; 32: 12673-12683.
[65] Narita T, Weinert BT and Choudhary C. Functions and mechanisms of non-histone protein acetylation. Nat Rev Mol Cell Biol 2019; 20: 156-174.
[66] Freireich EJ, Gehan EA, Rall DP, Schmidt LH and Skipper HE. Quantitative comparison of toxicity of anticancer agents in mouse, rat, hamster, dog, monkey, and man. Cancer Chemother Rep 1966; 50: 219-244.
[67] Strumberg D, Erhard J, Harstrick A, Klaassen U, Muller C, Eberhardt W, Wilke H and Seeber S. Phase I study of a weekly 1 h infusion of paclitaxel in patients with unresectable hepatocellular carcinoma. Eur J Cancer 1998; 34: 1290-1292.
[68] Shida T, Cueva JG, Xu Z, Goodman MB and Nachury MV. The major alpha-tubulin K40 acetyltransferase alphaTAT1 promotes rapid ciliogenesis and efficient mechanosensation. Proc Natl Acad Sci U S A 2010; 107: 21517-21522.
[69] Minucci S and Pelicci PG. Histone deacetylase inhibitors and the promise of epigenetic (and more) treatments for cancer. Nat Rev Cancer 2006; 6: 38-51.
[70] Lane AA and Chabner BA. Histone deacetylase inhibitors in cancer therapy. J Clin Oncol 2009; 27: 5459-5468.
[71] Saji S, Kawakami M, Hayashi S, Yoshida N, Hirose M, Horiguchi S, Itoh A, Funata N, Schreiber SL, Yoshida M and Toi M. Significance of

HDAC6 regulation via estrogen signaling for cell motility and prognosis in estrogen receptor-positive breast cancer. Oncogene 2005; 24: 4531-4539.

[72] Azuma K, Urano T, Horie-Inoue K, Hayashi S, Sakai R, Ouchi Y and Inoue S. Association of estrogen receptor alpha and histone deacetylase 6 causes rapid deacetylation of tubulin in breast cancer cells. Cancer Res 2009; 69: 2935-2940.

[73] Bae HJ, Jung KH, Eun JW, Shen Q, Kim HS, Park SJ, Shin WC, Yang HD, Park WS, Lee JY and Nam SW. MicroRNA-221 governs tumor suppressor HDAC6 to potentiate malignant progression of liver cancer. J Hepatol 2015; 63: 408-419.

[74] Elgendy M, Ciro M, Hosseini A, Weiszmann J, Mazzarella L, Ferrari E, Cazzoli R, Curigliano G, DeCensi A, Bonanni B, Budillon A, Pelicci PG, Janssens V, Ogris M, Baccarini M, Lanfrancone L, Weckwerth W, Foiani M and Minucci S. Combination of hypoglycemia and metformin impairs tumor metabolic plasticity and growth by modulating the PP2A-GSK3beta-MCL-1 axis. Cancer Cell 2019; 35: 798-815, e5.

[75] Kang MJ, Moon JW, Lee JO, Kim JH, Jung EJ, Kim SJ, Oh JY, Wu SW, Lee PR, Park SH and Kim HS. Metformin induces muscle atrophy by transcriptional regulation of myostatin via HDAC6 and Fox03a. J Cachexia Sarcopenia Muscle 2022; 13: 605-620.

Supplementary Table 1. Clinical information from TCPA database

Group	Subgroup	Ace-K40		Group	Subgroup	Ace-K40	
		Low	High			Low	High
Age	< 40	11	10	T Stage	1	41	30
	41~60	23	32		2	22	20
	> 60	56	47		3	22	34
Gender	Male	51	60		4	4	5
	Female	39	29		Unknown	1	0
Histological	Fibrolamellar Carcinoma	2	0	N Stage	0	83	81
	Hepatocellular Carcinoma	87	88		1	1	2
	Hepatocholangiocarcinoma	1	1		Unknown	6	6
Surgery	Extended Lobectomy	6	10	M Stage	0	85	83
	Lobectomy	31	42		1	1	1
	Segmentectomy, Single	14	10		Unknown	4	5
	Segmentectomy, Multiple	27	15		I	40	28
	Other (specify)	11	11		II	20	18
	Unknown	1	1		III*	2	1
Tumor Grade	G1	20	11	AJCC Grade	IIIA	18	27
	G2	36	46		IIIB	1	4
	G3	30	31		IIIC	2	4
	G4	0	1		IV*	0	1
	Unknown	4	0		IVB	1	0
Tumor Resist	R0	71	74	Vascular Invasion	Unknown	6	6
	R1	6	6		Macro	3	5
	R2	0	1		Micro	19	21
	RX	8	6		None	53	42
	Unknown	5	2		Unknown	15	21

*: III, IV represent those patients who do not have substage, apart from IIIA, IIIB, IIIC, IVB.

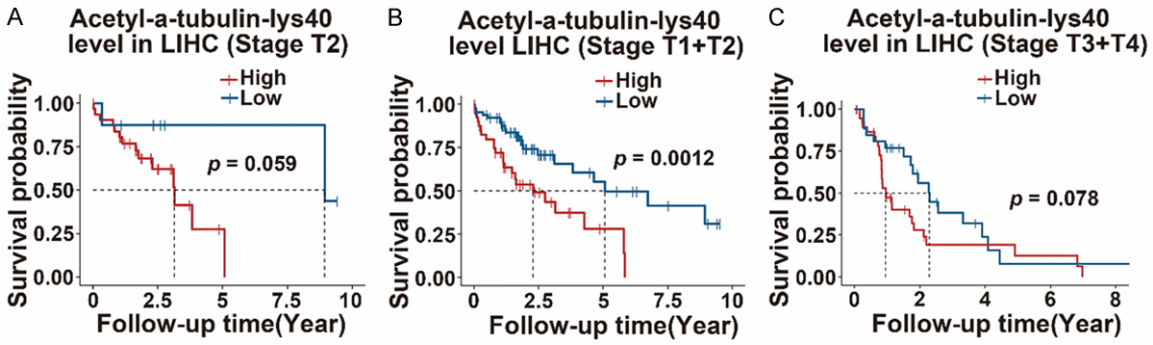

Supplementary Figure 1. A. Overall survival (OS) analysis was performed on acetyl-a-tubulin-lys40 for T2 stage HCC patients with a cutoff of -0.63572 and *P* = 0.059; B. Survival curve for T1+T2 (early stage) HCC patients with a cutoff of -0.20037 and *P* = 0.0012; C. Survival curve for T3+T4 stage (advanced stage) HCC patients with a cutoff of -0.23763 and *P* = 0.078.

Supplementary Table 2. Clinical information from Dongyang people's hospital

Group		Number	Group		Number
Gender	Male	52	Ace-K40	0	9
	Female	7		1+	8
Age	≤ 40	7		2+	29
	41~60	24		3+	11
	> 60	28		Loss	2
Surgery	Segmentectomy, Single	14	T Stage	1a	2
	Segmentectomy, Multiple	9		1b	43
	Lobectomy	11		2	3
	Extended Lobectomy	9		3	0
	Other (specify)	16		4	11
Histological differentiated	Poorly	2	N Stage	0	59
	Moderately to poorly	9		1	0
	Moderately	24	M Stage	0	59
	Well to moderately	7		1	0
	Well	5	AJCC Grade	2	3
	Unknown	12		1A	2
				1B	43
				3B	11

Supplementary Table 3. Univariate Cox regression of clinical patients

Group	Univariate Cox Regression		
	HR	CI95	P
Age	0.99	0.93-1.05	0.662
Histological	1.11	0.49-2.5	0.799
Acetyl-α-tubulin-lys40	2.62	0.62-11.02	0.188
Gender	0.84	0.1-6.85	0.872
T Stage	1.43	0.87-2.33	0.154

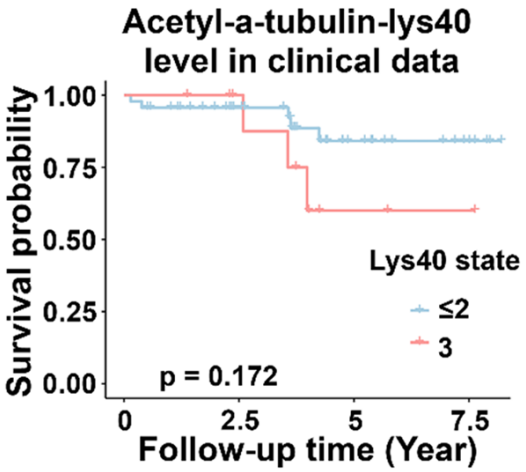

Supplementary Figure 2. The results of overall survival analysis for clinical cases, with acetyl-α-tubulin-lys40 level ≤ 2 as the low-level group, and acetyl-α-tubulin-lys40 level = 3 as the high-level group, showed a *p*-value of 0.172.

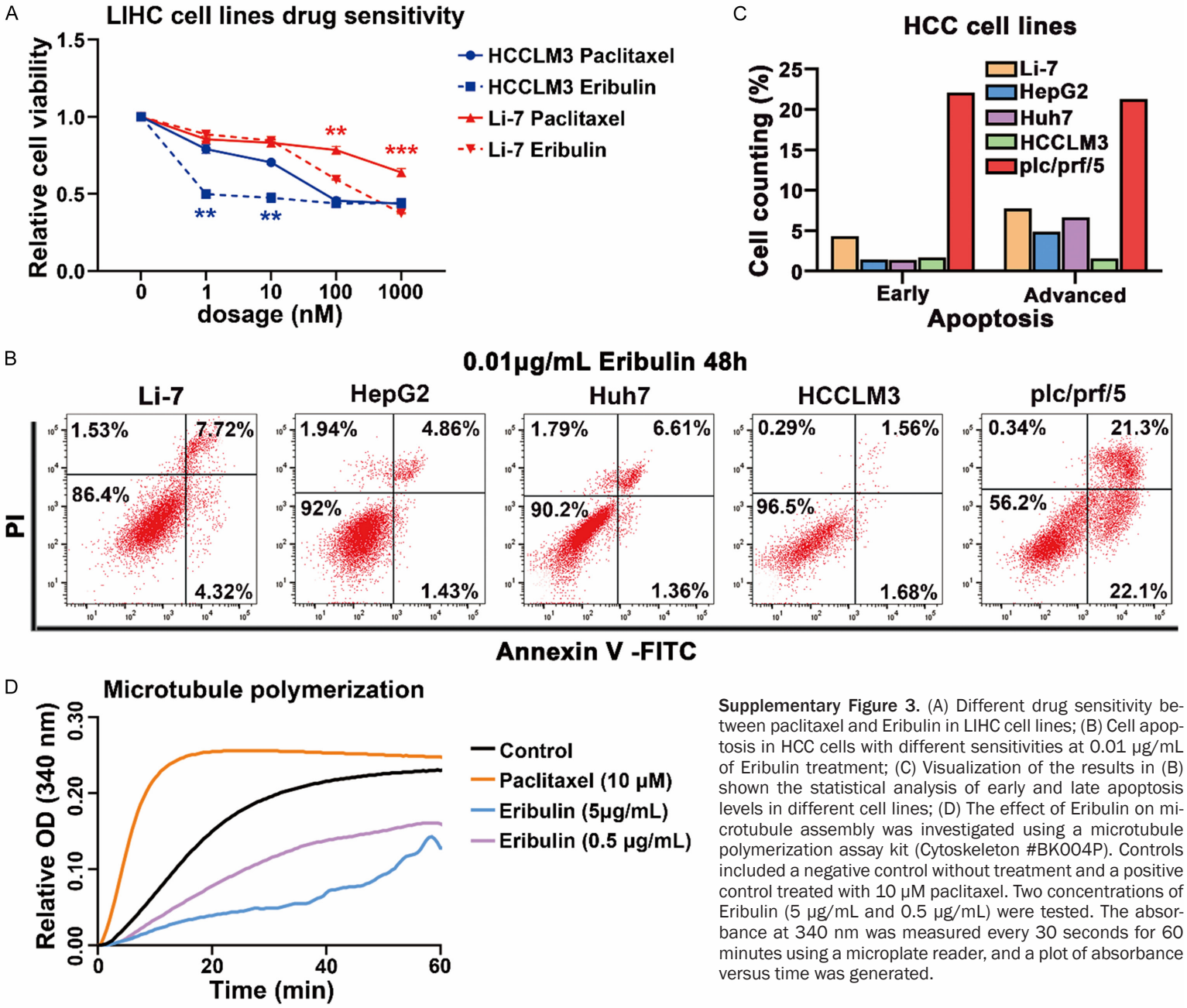

Supplementary Figure 3. (A) Different drug sensitivity between paclitaxel and Eribulin in LIHC cell lines; (B) Cell apoptosis in HCC cells with different sensitivities at 0.01 μg/mL of Eribulin treatment; (C) Visualization of the results in (B) shown the statistical analysis of early and late apoptosis levels in different cell lines; (D) The effect of Eribulin on microtubule assembly was investigated using a microtubule polymerization assay kit (Cytoskeleton #BK004P). Controls included a negative control without treatment and a positive control treated with 10 μM paclitaxel. Two concentrations of Eribulin (5 μg/mL and 0.5 μg/mL) were tested. The absorbance at 340 nm was measured every 30 seconds for 60 minutes using a microplate reader, and a plot of absorbance versus time was generated.

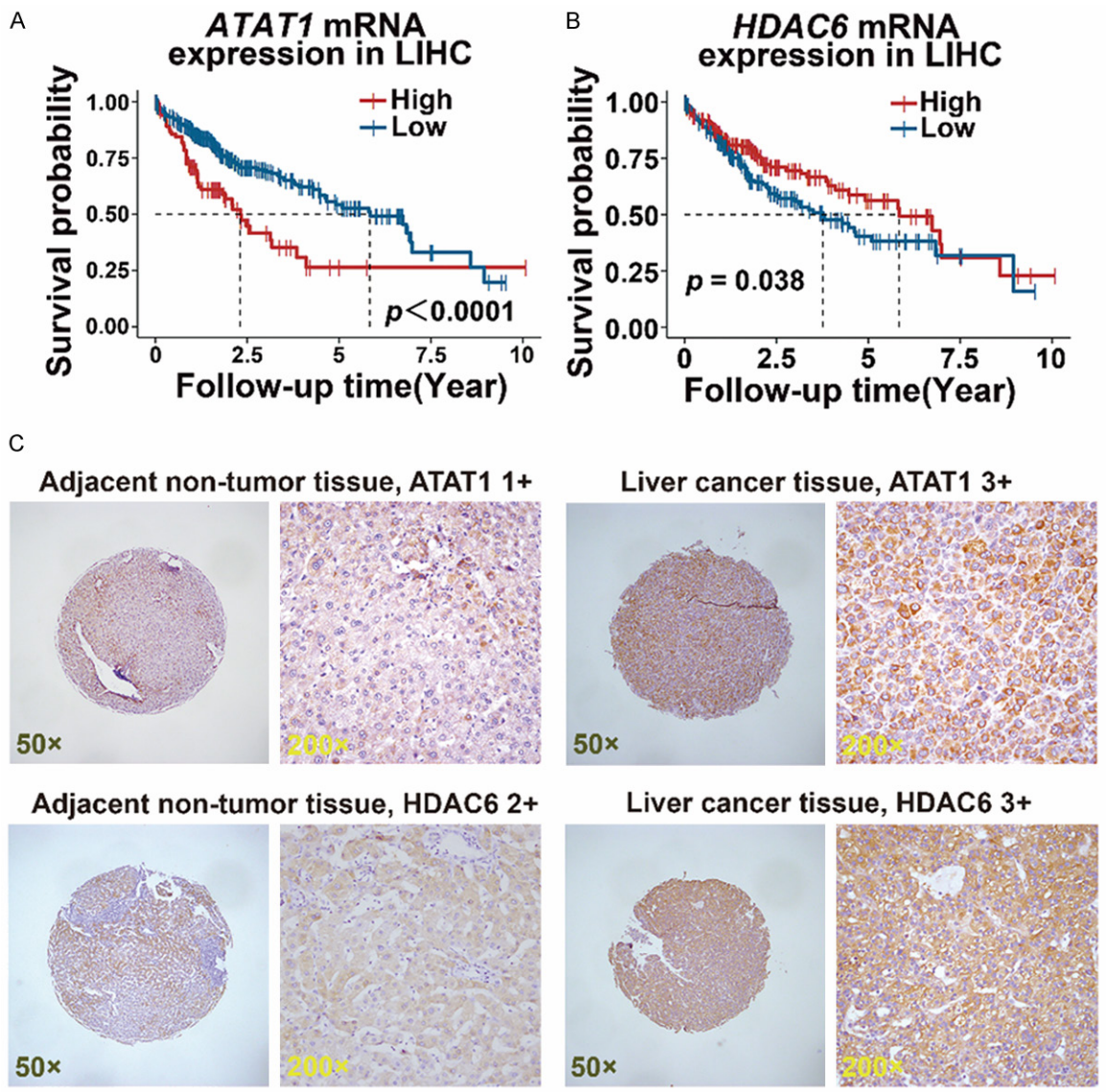

Supplementary Figure 4. A, B. The TPGA database was used to analyze the effect of mRNA levels of ATAT1 and HDAC6 on OS in HCC patients, with *p*-values of < 0.0001 and 0.038, respectively; C. Example of ATAT1 and HDAC6 immunohistochemical staining results on tissue microarray (TMA) (50 × and 200 × magnification for each group). The upper panel shows ATAT1 staining scored as 1+ in the adjacent non-tumor tissue (left) and 3+ in the HCC tissue (right). The lower panel shows HDAC6 staining scored as 2+ in the adjacent non-tumor tissue (left) and 3+ in the HCC tissue (right).

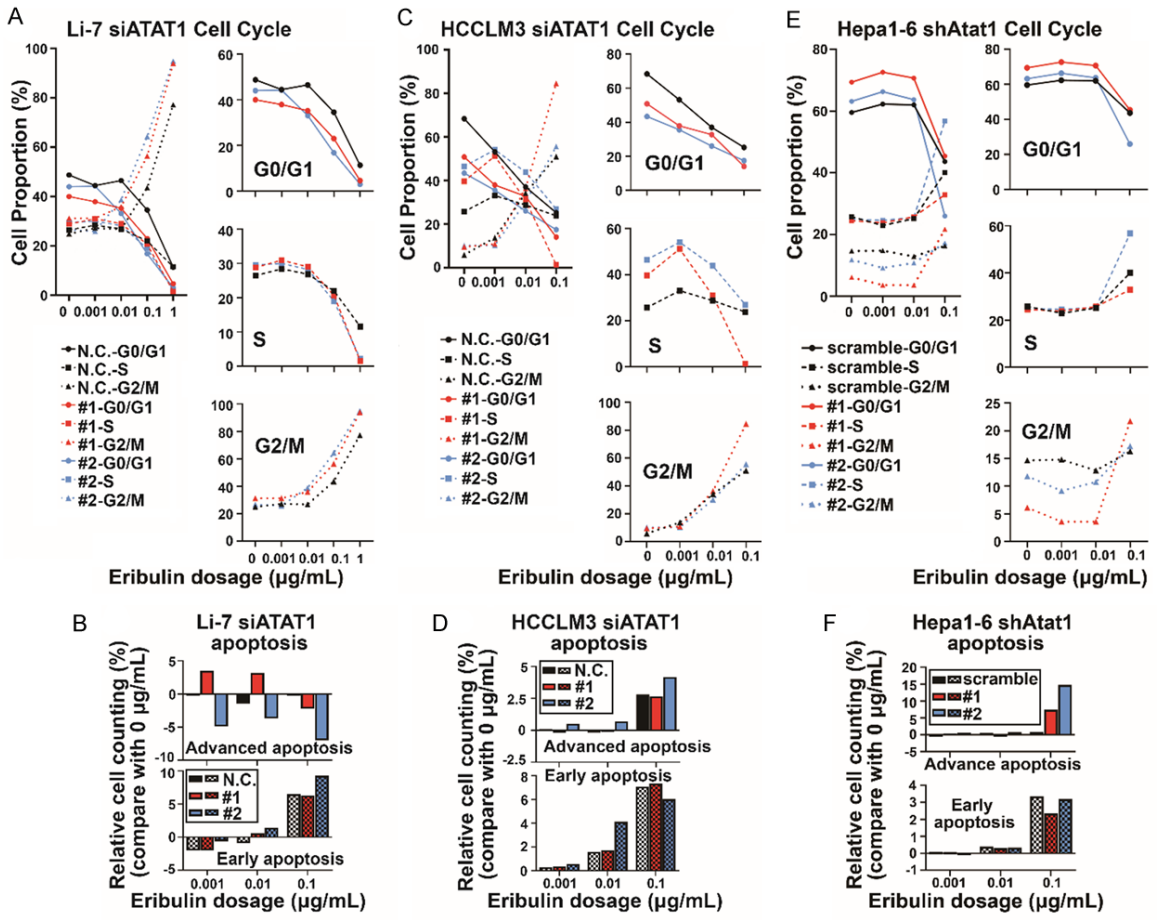

Supplementary Figure 5. A. Results of cell cycle analysis in ATAT1-knockdown Li-7 cells after treatment with Eribulin at different concentrations, with values on the vertical axis representing the absolute percentage of cells in each cell cycle phase; the sum of the percentage of G0/G1, S, and G2/M phase cells equals 100%; B. Results of cell apoptosis in ATAT1-knockdown Li-7 cells after treatment with Eribulin at different concentrations, with subtraction of the baseline (Eribulin 0 μg/mL) as reference and increment on the vertical axis representing the change in cell ratio; C, D. Data for ATAT1-knockdown HCCLM3 cell; E, F. Data for Atat1-knockdown Hepa1-6 cell.

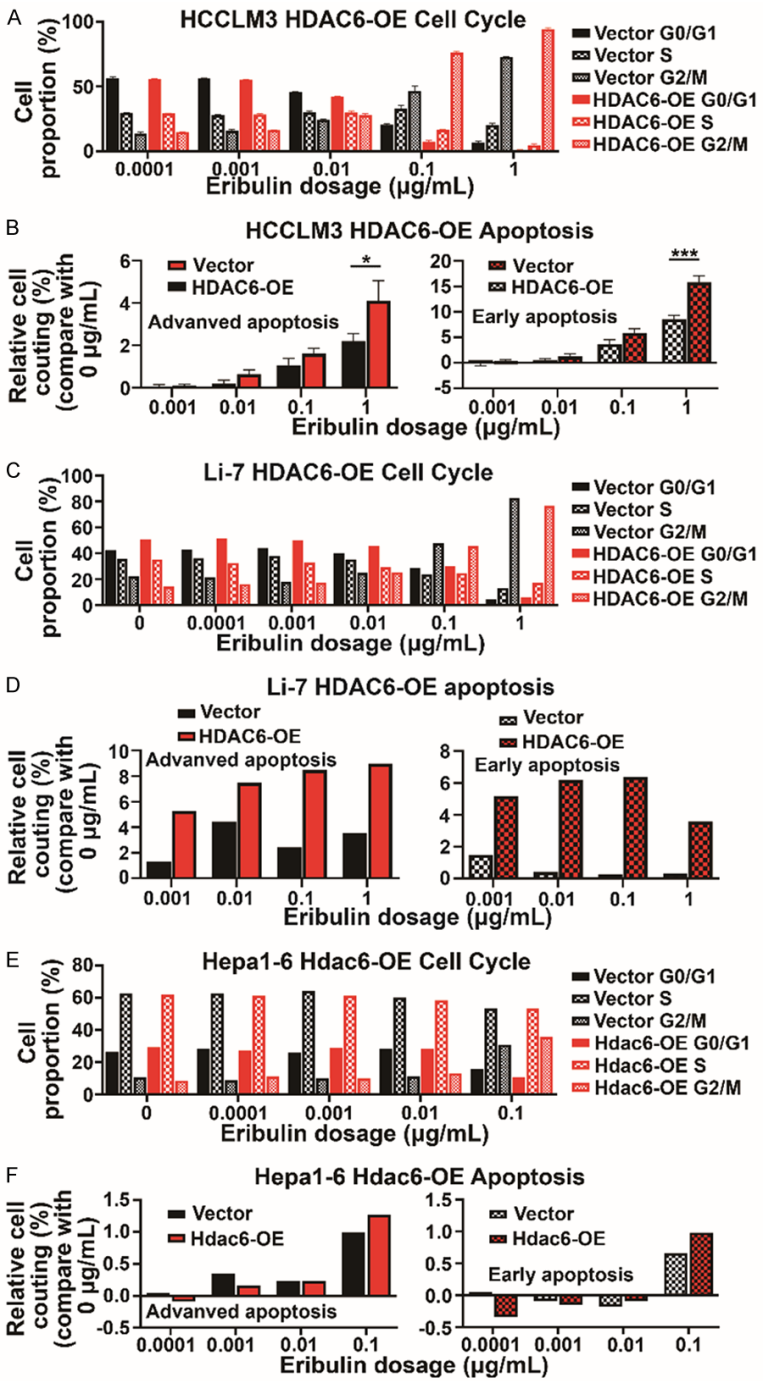

Supplementary Figure 6. A. Results of cell cycle analysis in HDAC6-OE HCCLM3 cells after treatment with Eribulin at different concentrations, with values on the vertical axis representing the absolute percentage of cells in each cell cycle phase; the sum of the percentage of G0/G1, S, and G2/M phase cells equals 100%; B. Results of cell apoptosis in HDAC6-OE HCCLM3 cells after treatment with Eribulin at different concentrations, with subtraction of the baseline (Eribulin 0 μg/mL) as reference and increment on the vertical axis representing the change in cell ratio; C, D. Data for HDAC6-OE Li-7 cell; E, F. Data for Hdac6-OE Hepa1-6 cell.

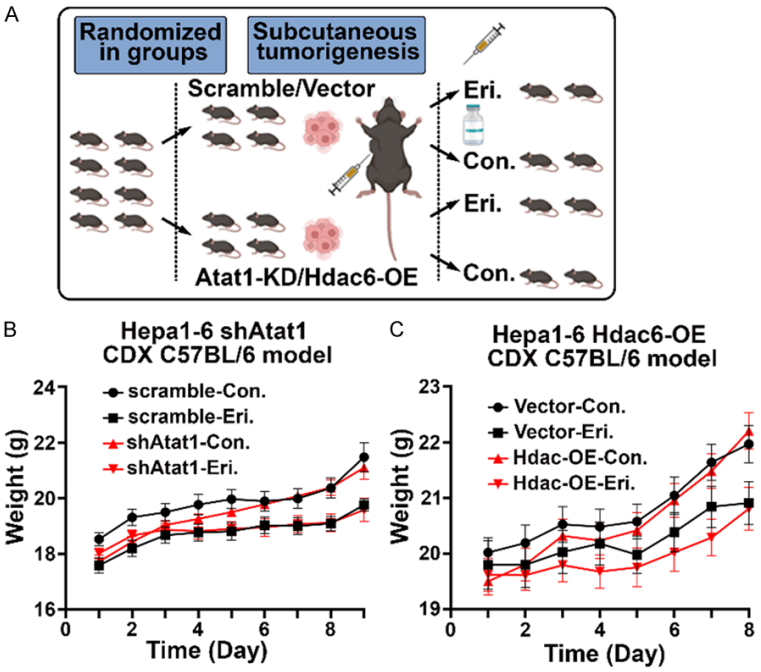

Supplementary Figure 7. A. Mice experimental procedure diagram; B. Weight curve of experimental mice with Atat1 knockdown; C. Weight curve of experimental mice with Hdac6 overexpression.